Testosterone acts through membrane protein GPRC6A to cause cardiac edema in zebrafish embryos

Vahid Zadmajid, Shayan Shahriar & Daniel A. Gorelick

Center for Precision Environmental Health
Department of Molecular & Cellular Biology
Baylor College of Medicine
One Baylor Plaza, BCM229
Houston, Texas 77030
USA

Correspondence to DAG: gorelick@bcm.edu

Abstract

Androgen actions are classically thought to be mediated by intracellular androgen receptors (AR), but they can also exert non-genomic effects via binding to integral membrane proteins. Although several putative membrane androgen receptors were cloned and characterized *in vitro*, their function as androgen receptors *in vivo* remains to be further investigated. Here, we used a chemical-genetic screen in zebrafish and found that the G-protein coupled receptor GPRC6A mediates non-genomic androgen action during embryonic development. Exposure to three androgens, 5α-Androstane-3,17-dione (androstanedione), dihydrotestosterone (DHT), and testosterone, caused cardiac edema or tail curvature in wild-type embryos. *ar* mutant embryos also exhibited cardiac edema or tail curvature following exposure to these androgens, suggesting the involvement of *ar*-independent pathways. To identify the causative receptor, we mutated putative membrane androgen receptors *gprc6a*, *hcar1-4*, or *zip9* genes and exposed mutant embryos to the androgens. We found that *hcar1-4* and *zip9* mutant embryos were susceptible to the identified androgens and developed cardiac edema or tail curvature phenotype following exposure. In contrast, we observed a significant reduction in cardiac edema phenotype in the *gprc6a* mutants compared to the wild-type embryos following testosterone treatment. Additionally, we exposed wild-type embryos to testosterone together with GPRC6A antagonists and observed a significant suppression of the cardiac edema phenotype. These results suggest that testosterone causes cardiac edema in zebrafish embryos by acting via the integral membrane protein GPRC6A, independently of nuclear androgen receptors. Using RNA-seq and RNA rescue approaches, we find that testosterone-GPRC6A causes cardiac phenotypes by

reducing Pak1 signaling. Our study provides insights into non-genomic androgen signaling during embryonic development and identifies GPRC6A as a key receptor mediating androgen action.

48 **Introduction**

49 Androgens regulate the development and function of multiple tissues and cell
50 types, including muscle, heart, bone, skin, prostate, reproductive tract, and the brain
51 (Bakker, 2022; Cunha et al., 2017; Murashima et al., 2015; Rossetti et al., 2017).
52 Classically, androgens act by binding to cytosolic androgen receptors (AR), ligand-
53 inducible transcription factors (Chang et al., 1988; Lubahn et al., 1988a; Lubahn et al.,
54 1988b; Tilley et al., 1989; Trapman et al., 1988). Androgens can also activate signal
55 transduction pathways independently of transcription, via a mechanism called non-
56 genomic signaling (Gorczynska and Handelsman, 1995). These rapid androgen actions
57 can be mediated by second messenger signaling pathways such as activation of
58 intracellular kinases (eg MAPK, PI-3K) or increases in intracellular Ca^{2+} (Estrada et al.,
59 2003; Gatson and Singh, 2007; Gatson et al., 2006; Guo et al., 2002; Kang et al., 2004;
60 Lieberherr and Grosse, 1994; Liu et al., 2022). Androgen signaling occurs in the
61 absence of nuclear AR (Guo et al., 2002; Hatzoglou et al., 2005; Pi et al., 2010). Such
62 non-genomic androgen signaling has been observed in different cell types, including T
63 cells and macrophages (Benten et al., 1999; Wunderlich et al., 2002), osteoblasts (Kang
64 et al., 2004; Lieberherr and Grosse, 1994), prostate and breast cancer cells (Hatzoglou
65 et al., 2005; Liu et al., 2015; Sun et al., 2006), granulosa and Sertoli cells (Gorczynska
66 and Handelsman, 1995; Machelon et al., 1998), and skeletal muscle (Estrada et al.,
67 2000). However, the receptors that mediate non-genomic androgen signaling are not
68 well understood.

69 Several putative membrane androgen receptors such as G protein-coupled
70 receptor family C group 6 member A (GPRC6A) (Pi and Quarles, 2012; Pi et al., 2008;

71 Pi et al., 2010), the zinc transporter member 9 protein (ZIP9/SLC39A9) (Thomas et al.,
72 2014), the G protein-coupled oxo-eicosanoid receptor 1 (OXER1) (Kalyvianaki et al.,
73 2017), and ion channels such as transient receptor potential melastatin 8 (TRPM8)
74 (Asuthkar et al., 2015a; Asuthkar et al., 2015b), or L-type Ca^{2+} channel, Cav1.2 (Scragg
75 et al., 2004; Scragg et al., 2007) were identified based on their ability to bind androgens
76 *in vitro*.

77 However, the evidence for androgen-dependent function of such proteins *in vivo*
78 is less clear, in part because receptors have multiple ligands. For example, zebrafish
79 *zip9* mutants exhibited reduced fecundity and egg viability compared with wild-type
80 (Converse and Thomas, 2020) while mouse and zebrafish with mutations in *Cav1.2*
81 exhibited cardiac abnormalities (Fu et al., 2011; Rosati et al., 2011; Rottbauer et al.,
82 2001; Seisenberger et al., 2000), but whether these phenotypes are influenced by
83 androgens, or other ligands binding to these receptors, is not known.

84 Here, we describe an *in vivo* screening approach combining chemical exposures
85 and CRISPR/Cas9 genome editing in zebrafish embryos to discover membrane
86 androgen receptors. Using this approach, we discovered that exposure to exogenous
87 testosterone alters cardiac development in zebrafish embryos, and that this occurs via
88 GPRC6A, independently of nuclear AR. We provide evidence that testosterone, and not
89 a metabolite, acts via GPRC6A. We also discovered that exposure to two additional
90 androgens, androstanedione and dihydrotestosterone, cause developmental
91 phenotypes in zebrafish, independently of nuclear AR, GPRC6A, ZIP9 or OXER1,
92 suggesting that additional membrane androgen receptors exist and influence embryonic
93 development.

Materials and Methods

Zebrafish

Zebrafish were raised at 28.5°C on a 14-h light, 10-h dark cycle in the Baylor College of Medicine (BCM) Zebrafish Research Facility in a recirculating water system (Aquaneering, Inc., San Diego, CA) and a Tecniplast recirculating water system (Tecniplast USA, Inc., West Chester, PA). Wild-type zebrafish were AB strain (Westerfield, 2000) and all mutant lines were generated on the AB strain. The following previously published mutant and transgenic lines were used: nuclear androgen receptor *ar* ^{uab142} (Crowder et al., 2018), estrogen receptor mutants *esr1a* ^{uab118} (ERα), *esr2a* ^{uab134} (ERβ1), *esr2b* ^{uab128} (ERβ2) (Romano et al., 2017), and *Tg(myl7:EGFP)*(Huang et al., 2003). All procedures were approved by the BCM Institutional Animal Care and Use Committee.

Embryo collection

Adult zebrafish were allowed to spawn naturally in pairs or in groups. Embryos were collected during 20 minute intervals to ensure precise developmental timing within a group. Embryos were placed in 60 cm^2 Petri dishes at a density of no more than 100 per dish in E3B media (60X E3B: 17.2g NaCl, 0.76g KCl, 2.9g $CaCl_2$-$2H_2O$, 2.39g $MgSO_4$ dissolved in 1 L Milli-Q water; diluted to 1X in 9 liter Milli-Q water plus 100 µL 0.02% methylene blue), and then stored in an incubator at 28.5°C. Between 24- and 48-hours post fertilization (hpf), embryos were manually dechorionated.

117 **Embryo treatments**

118 At 2-4 hpf, embryos were incubated in E3B with androgen receptor modulator(s) or
119 estradiol at 28.5°C until imaging or RNA extraction at 3 dpf. Dead embryos were
120 removed daily. Embryos that were alive but abnormal were left in the dish and
121 recorded. We did not observe any significant mortality differences between the
122 treatments and vehicle control. All chemicals were purchased as follows:
123 androstanedione CAS registry number 846-46-8, Isosciences catalog # 13386, purity ≥
124 95%; dihydrotestosterone CAS 521-18-6, Isosciences catalog # 6065UNL, purity ≥ 98%;
125 testosterone CAS 58-22-0, Sigma catalog # T1500, purity ≥ 98%; calindol CAS #
126 29610-18-8, Sigma catalog # SML1386, purity ≥ 98%; NPS-2143, CAS # 324523-20-8,
127 Sigma catalog # SML0362, purity ≥ 98%; epigallocatechin gallate, CAS # 989-51-5,
128 Sigma catalog # E4143, purity = 99.87%; estradiol, CAS # 50-28-2, Sigma catalog #
129 E8875, purity ≥ 98%. All chemical stocks were made in 100% DMSO at 1000x and
130 diluted in E3B embryo media to the final concentration (1x) at the time of treatment. All
131 vehicle controls are 0.1% DMSO.

132

133 **CRISPR-Cas9 mutant generation**

134 Chemically synthesized gRNAs for *gprc6a*, *zip9*, *oxer1* (*hcar1-4*), *cav1.2*, and purified
135 Cas9 protein were obtained from Synthego (Redwood City, CA, USA). The target
136 sequences were identified using CHOPCHOP (Labun et al., 2021) or zebrafish genome-
137 scale lookup table from Wu et al. (Wu et al., 2018). Target site sequences are shown in
138 Table S1. 1-cell-stage embryos were injected using glass needles pulled on a Sutter
139 Instruments Fleming/Brown Micropipette Puller, model P-97, and a regulated air-

140 pressure micro-injector (Harvard Apparatus, New York, PL1–90). Each embryo was
141 injected with a 1 nl solution containing 1 µl of 10µM gRNA, 1 µl of 20µM Cas9 protein, 2
142 µl of 1.5 M KCl, 1 µl phenol red. The mixture was filled to 10 µL with 1X microinjection
143 buffer (10mM Tris-HCL, 0.1mM EDTA, pH 8.0 in nuclease-free H_2O) and incubated at
144 37 °C for 5-7 min before injection as described (Burger et al., 2016).
145
146 To generate *cyp19a1b* mutants, we hybridized oligonucleotides (oligo 1 5'-
147 TAGGAGCATGTGGTAAAGGATG, oligo 2 5'-AAACCATCCTTTACCACATGCT) to
148 generate double-stranded target DNA and annealed the DNA into digested pT7-gRNA
149 plasmid. pT7-gRNA plasmid was digested simultaneously with BsmBI, BglII and SalI for
150 one hour at 37 ^{o}C followed by one hour at 55 ^{o}C. gRNAs were synthesized and purified
151 from this plasmid template using in vitro transcription (MegaShortScript T7 kit, Life
152 Technologies). Cas9 mRNA was generated using in vitro transcription (mMessage
153 mMachine T3 kit, Life Technologies) from a linearized pT3TS-nCas9n plasmid. RNA
154 was purified using RNA clean & concentrator kit (Zymo Research). Plasmids pT7-gRNA
155 and pT3TS-nCas9n were obtained from Addgene (numbers 46759, 46757)(Jao et al.,
156 2013). Embryos were injected with a 1 nl solution containing 150 ng/µl of Cas9 mRNA,
157 50 ng/µl of gRNA and 0.1% phenol red.
158
159 For all gRNAs, mixtures were injected into the yolk of each embryo. Injected embryos
160 were raised to adulthood and crossed to wild-type fish (AB strain) to generate F1
161 embryos. F1 offspring were sequenced via tail fin biopsies to identify mutations
162 predicted to cause loss of functional protein.

163

164 **Genomic DNA isolation**

165 Individual embryos or tail biopsies from individual adults were placed in 100 µL ELB (10
166 mM Tris pH 8.3, 50 mM KCl, 0.3% Tween 20) with 1 µL proteinase K (800 U/ml, NEB) in
167 96 well plates, one sample per well. Samples were incubated at 55°C for 2 hours
168 (embryos) or 8 hours (tail clips) to extract genomic DNA. To inactivate Proteinase K,
169 plates were incubated at 98°C for 10 minutes and stored at -20°C.

170

171 **High resolution melt curve analysis**

172 PCR and melting curve analysis was performed as described (Parant et al., 2009). PCR
173 reactions contained 1 µl of LC Green Plus Melting Dye (BioFire Diagnostics), 1 µl of Ex
174 Taq Buffer, 0.8 µl of dNTP Mixture (2.5 mM each), 1 µl of each primer (5 µM), 0.05 µl of
175 Ex Taq (Takara Bio Inc), 1 µl of genomic DNA, and water up to 10 µl. PCR was
176 performed in a Bio-Rad CFX96 thermal cycler, using black/white 96 well plates (Bio-Rad
177 HSP9665). PCR reaction protocol was 98°C for 1 min, then 34 cycles of 98°C for 10
178 sec, 60°C for 20 sec, and 72°C for 20 sec, followed by 72°C for 1 min. After the final
179 step, the plate was heated to 95°C for 20 sec and then rapidly cooled to 4°C. Melting
180 curves were generated with a Bio-Rad CFX96 Real-Time System over a 70–95°C range
181 and analyzed with Bio-Rad CFX Manager 3.1 software. All mutations were confirmed by
182 TA cloning and sequencing. PCR primer sequences are shown in Table S2.

183

184 **ELISA testosterone uptake assay**

185 At 2-4 hpf, embryos were incubated in E3B with testosterone (30 μM) or vehicle
186 controls (0.1% DMSO) at 28.5°C until 3 dpf. Embryos were collected at 3 dpf and
187 transferred into 10 cryovials (Genesee Scientific, Cat #: 14-125) using a pipette (for
188 each treatment 50 embryos were pooled and placed in each 1.5 mL cryovial). E3B
189 media was aspirated out by pipetting (by immersing the pipette tips just below the
190 liquid's surface). Then, the embryos were washed 4 times using 1 ml 1X PBS, the
191 media was aspirated out and the samples were frozen overnight at -80 ◦C. Embryos
192 were thawed on ice and were homogenized in 200 μL of 1X PBS using a hand pellet
193 pestle homogenizer (Genesee Scientific, Cat #: 27-118) and stored overnight at -20°C.
194 After two additional freeze-thaw cycles to break the cell membranes (2 hours at -20°C
195 and 10 minutes on ice), the homogenates were centrifuged for 10 minutes at 10000 x g,
196 4°C to collect the supernatant. The supernatant was dried in a vacuum evaporator
197 (Thermo Scientific SpeedVac DNA130) and resuspended in 20 μL of 0.5%
198 trifluoroacetic acid (TFA) in 5% acetonitrile (ACN) before processing with Pierce™ C18
199 Spin Columns (Thermo Scientific™, Cat #: 89870). Each column was activated with 200
200 μL of 50% ACN and centrifuged at 1,500 x g for 1 minute. The columns were
201 equilibrated with 200 μL of 0.5% TFA, 5% ACN, and centrifuged at 1,500 x g for 1
202 minute. The full 20 μL samples were loaded on top of the resin bed in the column and
203 centrifuged at 1,500 x g for 1 minute. The columns were washed by adding 200 μL of
204 0.5% TFA in 5% ACN and centrifuged at 1,500 x g for 1 minute. 20 μL of elution buffer
205 (70% ACN) was added to the top of the resin bed and the columns were centrifuged at
206 1,500 x g for 1 minute. Finally, the samples were dried in a vacuum evaporator and
207 resuspended in 200 μL of 1X PBS. Testosterone levels were quantified using ELISA kits

208 according to the manufacturer (Cusabio Biotech, Cat #: CSB-E17554Fh). A serial
209 dilution factor test was run for 1X, 100X, 500X, 1000X, and 2000X samples so that the
210 concentration of testosterone in each sample was within the assay detection range (0.1
211 – 20 ng/mL). A standard curve was generated by measuring serially diluted standards
212 provided by the manufacturer (S0 = 0 ng/mL; S1 = 0.1 ng/mL; S2 = 0.4 ng/mL; S3 = 1.6
213 ng/mL; S4 = 5 ng/mL; S5 = 20 ng/mL). Mean absorbance readings for each standard (in
214 duplicate) were plotted on the x-axis against the concentration on the y-axis to draw a
215 best-fit curve through the points on the graph using Excel (Harris Model: y=1/(a+bx^c); r
216 = 0.99965). Samples were run in duplicate. Briefly, 50 µl of each sample, 50 µl of T-
217 horseradish peroxidase conjugate (HRP-conjugate), and 50 µl of antibody were
218 dispensed in each well of a 96-well plate and incubated for 1 hour at 37°C. After
219 aspirating each well and 3 washes (400 µl per well using manufacturer's 1X wash
220 buffer), 50 µl of manufacturer's substrate A and 50 µl of substrate B were added to each
221 well. The plate was then incubated for 15 min at 37°C in the dark and the reaction was
222 stopped by adding 50 µl of stop solution (1 N H_2SO_4). The optical density was read
223 within 10 minutes at 450 nm with a microtiter plate reader (Cytation™ 5 Cell Imaging
224 Multi-Mode Reader, Biotek, USA) and BioTek Gen5 Software. ELISA data of samples
225 were interpolated from the standard curve generated by Excel to calculate the
226 concentrations of target samples using the ELISA data analysis guide provided by
227 CUSABIO (https://www.cusabio.com/m-225.html). Testosterone is presented as ng/ml.
228 To calculate the amount of testosterone per embryo, we divided the total concentration
229 of testosterone in the pooled embryos by 50. The detection limit of testosterone was 0.1
230 ng/ml, with sensitivity 0.05 ng/mL, according to the manufacturer.

231

232 **Live imaging**

233 Embryos were imaged with a Nikon SMZ25 microscope equipped with a Hamamatsu
234 ORCA-Flash4.0 digital CMOS camera, or with a Nikon SMZ18 microscope equipped
235 with a Nikon DS-Fi3 camera. Images were equally adjusted for brightness and contrast
236 in Adobe Photoshop Creative Cloud. For imaging of embryos following chemical
237 exposure, embryos were imaged in E3B in 60 mm^2 dishes in 0.04% tricaine anesthetic.
238 For embryos in a mixed clutch containing multiple genotypes, embryos were genotyped
239 following imaging using high resolution melting curve analysis. For confocal microscopy,
240 embryos were anesthetized in E3B with 0.04% tricaine, positioned ventrally in 0.8% low-
241 melt agarose in E3B on glass cover slips and imaged on a Nikon Ti2-E inverted
242 microscope with Yokogawa CSU-W1 spinning disk confocal and Photometrics
243 Prime95b sCMOS camera. Images were captured and maximum intensity projections
244 were created using Nikon NIS-Elements-AR v5.42.03. Images were adjusted for
245 brightness/contrast using FIJI (Schindelin et al., 2012).

246

247 **RNA Extraction and RNAseq Sample Preparation**

248 Starting at 2-4 hpf, embryos were incubated in E3B with testosterone, testosterone +
249 EGCG, testosterone + calindol and 0.1% DMSO (vehicle control) at 28.5°C until RNA
250 extraction at 3 dpf. Dead embryos were removed daily. In both testosterone and
251 testosterone + calindol (T+calindol) treated groups, embryos that exhibited cardiac
252 phenotypes were pooled and selected for RNAseq. In the testosterone + EGCG
253 (T+EGCG) treated groups, embryos that exhibited normal phenotypes were pooled and

254 selected for RNAseq. All DMSO-treated embryos were normal. Treated embryos (20 per
255 group) were transferred into RNAse-free tubes (Thermo-Scientific™ Snap Cap Low
256 Retention Microcentrifuge Tubes, catalog #3434). Embryos were euthanized by placing
257 the tube in ice and residual E3 media was withdrawn using 27 G x 1.25 inch BD
258 PrecisionGlide™ Needle (catalog #305109). 200uL Trizol reagent (Thermo-scientific,
259 catalog #15596026) was added to each tube containing treated embryos followed by
260 homogenization with a motorized pestle. After that, an additional 800uL Trizol was added
261 per tube, vortexed, and incubated at room temperature for 5 minutes. Tubes were
262 centrifuged at 12000G for 10 minutes at 4°C. Then, we transferred the supernatant to
263 fresh tubes and stored them at -80°C overnight. Frozen embryo lysates were thawed on
264 ice the next day. We used the Direct-zol RNA miniprep Kit from Zymo Research (catalog
265 #11-331) and followed the manufacturer protocol to extract RNA. RNA quality control
266 analysis was performed using NanoDrop 1000 (Thermo-scientific) and Agilent 4200
267 TapeStation System. Good quality RNA with 260/280 absorbance of 2.0 or more and RIN
268 value of 9.0 or more was sent for Directional mRNA library preparation (poly A
269 enrichment) and NovaSeq X Plus Series (paired-end, 150 basepair max read length)
270 sequencing by Novogene America.
271
272 **RNA Sequencing Analysis**
273 Data analysis was performed on the high-performance computing (HPC) cluster that is
274 managed by the Biostatistics and Informatics Shared Resource (BISR) at the Baylor
275 College of Medicine. We trimmed the raw RNA sequencing FastQ data for low-quality
276 reads using trim_galore (version 0.6.10) (Krueger, 2015), and then mapped them using

277 STAR (version 2.7.1a) (Dobin et al., 2013) onto the zebrafish genome assembly
278 GRCz11, maintained by the Genome Reference Consortium (GRC). Mapped sequence
279 reads were aligned to genomic features using featureCounts (Liao et al., 2014).
280 Combined genomic features were normalized using upper-quartile (UQ) and Remove
281 Unwanted Variation method (Risso et al., 2014). Differentially expressed genes (DEGs)
282 were determined using the EdgeR R package (Robinson et al., 2010). We made a
283 separate list of DEGs (FDR < 0.05) for each treatment group (testosterone, testosterone
284 + EGCG, testosterone + calindol) by comparing their genomic features with the genomic
285 features of the control group treated with 0.1% DMSO. After that, we made a list of T-
286 GPRC6A-specific genes (testosterone-GPRC6A-specific genes) by combining the
287 significant genes that are differentially expressed in one direction (upregulated or
288 downregulated in terms of fold change) in both testosterone and T+calindol treated
289 groups but get rescued in the T+EGCG treated group by either showing no fold change
290 or fold change in the opposite direction (e.g. if genes are upregulated in T, they will be
291 downregulated in T+EGCG or vice versa) or 50% reduced fold change in the same
292 direction (e.g. if up/downregulation (T) = 2x, up/downregulation (T+EGCG) ≤ x).
293 GOBP (Gene Ontology Biological Process) pathway enrichment was performed using
294 GSEA-v3.0 (https://www.gsea-msigdb.org/gsea/downloads.jsp) (Mootha et al., 2003;
295 Subramanian et al., 2005). Any pathway with an adjusted FDR value <0.25 was
296 considered significant. All RNA-seq data is deposited in the GEO repository, accession
297 number GSE274852.
298
299 **Rescue experiment**

300 CMV vectors (pTwist CMV) incorporating the open reading frame of either *pak1* or *grk3*
301 were constructed by Twist Bioscience (San Francisco, CA, USA). All plasmids were
302 sequenced prior to experimentation by Plasmidsaurus (Oregon, USA). Plasmids
303 containing either *pak1* or *grk3* were linearized by the restriction enzyme NotI (NEB
304 R3189S). mRNA was transcribed using the mMessage mMachine SP6 Kit (Invitrogen,
305 AM1340) and purified with the RNA clean & concentration kit (Zymo Research, R1019).
306 Embryos were microinjected at the one-cell stage with 1 nl total volume containing
307 either *pak1* or *grk3* (30 pg mRNA) or *GFP* mRNA (50 pg mRNA). All solutions were
308 injected into the yolk.
309
310 **Experimental design and data analysis**
311 Each experiment included comparing groups (treated vs untreated or mutant vs
312 wildtype) using 11-160 embryos per group with all embryos from the same clutch.
313 Experiments were performed on 3-6 clutches for each genotype. This is essentially a
314 complete block design with clutch as block. Mean cardiac edema or tail curvature rate of
315 individual embryos from a clutch was used for comparing treatment groups (or mutant
316 groups) within experiments using one-way ANOVA with Tukey's multiple comparisons
317 test. For some individual pairs of comparisons, paired t test was used. Significance level
318 is 0.05. All Statistical analyses were performed using Prism version 9.4.1 (GraphPad
319 Software, Boston, MA).
320

321 **Results**

322

323 **Strategy to identify membrane androgen receptors using genetic and**

324 **pharmacologic approaches**

325 The strategy we adopted is shown schematically in Fig. 1. We exposed wild-type
326 embryos to multiple androgens at different concentrations (10-100 μM) in embryo
327 media, beginning at 3 hours post fertilization. We assayed embryo morphology at 2- and
328 3- days post fertilization (see Materials and Methods). We identified three androgens,
329 5α-Androstane-3,17-dione (androstanedione) (15 μM), dihydrotestosterone (DHT) (30
330 μM), and testosterone (30 μM), that caused a morphologic abnormality. All three
331 compounds caused cardiac edema with elongated and incompletely looped hearts (Figs
332 2 and S1, Table 1; androstanedione mean embryos with cardiac edema 84% ± 12%
333 standard deviation, DHT 96% ± 6%, testosterone 79% ± 4%, n=6 clutches, 15-27
334 embryos per clutch). Additionally, androstanedione and DHT, but not testosterone,
335 caused a tail curvature phenotype in which the caudal tail was curved dorsally
336 (androstanedione mean embryos with tail curvature 94% ± 5% standard deviation, DHT
337 81% ± 20). For embryos exposed to androstanedione or DHT, every embryo that
338 exhibited cardiac edema also exhibited a tail curvature phenotype (Table 1). Other
339 features of embryos, like gross morphology of the head, eyes, somites, otolith,
340 notochord, brain ventricles, fin folds, and yolk, appeared normal, suggesting that these
341 androgens affect specific developmental processes and do not cause generalized, non-
342 specific toxicity.

343

344 **Neither androstanedione, DHT, nor testosterone act via nuclear androgen**
345 **receptor (*ar*) to cause morphologic phenotypes in zebrafish embryos**

346 To explore whether these three androgens act via nuclear *ar* to cause
347 morphologic phenotypes, we crossed heterozygous *ar* $^{uab142/+}$ zebrafish to each other
348 and exposed the resulting embryos to vehicle (0.1% DMSO), androstanedione, DHT, or
349 testosterone beginning at 3 hours post fertilization. Following chemical exposure, we
350 observed no statistically significant difference in the percent of embryos exhibiting
351 cardiac edema or tail curvature phenotypes between wild-type, heterozygous *ar* $^{uab142/+}$,
352 or homozygous *ar* $^{uab142/uab142}$ embryos (Fig. 2, Table 1). We conclude that zebrafish
353 embryos with mutations in nuclear *ar* are sensitive to androstanedione, DHT, or
354 testosterone exposure, which raises the possibility that these androgens act via an *ar*-
355 independent pathway to cause morphologic phenotypes during embryonic development.
356

357 **Quantification of testosterone uptake in zebrafish**

358 Our androgen exposure concentrations in fish water (30 μM) is higher than the
359 dissociation constant (Kd) for testosterone binding to the zebrafish nuclear *ar* (2
360 nM)(Jørgensen et al., 2007). However, it is not known how much of the androgen in the
361 water is absorbed and bioavailable in the zebrafish embryo. We used ELISA to measure
362 the amount of testosterone in zebrafish following exposure to water containing 30 μM
363 testosterone from 0 to 3 dpf. We found that the testosterone concentration in the whole
364 embryo was 65.90 ± 33.93 nM/per embryo (mean ± SD, Fig. 3). While this is ~30 fold
365 more than Kd for testosterone binding to the zebrafish AR/NR3C4 (2 nM), these levels
366 are more similar to physiologic levels of circulating testosterone in adult human men

367 (10-30 nM) (Burger, 2002; Finkelstein et al., 2013; Kelsey et al., 2014; Mohr et al., 2005;
368 Travison et al., 2017; Wu et al., 2010). Moreover, this estimation does not consider the
369 percent of androgens that are bioavailable or bound to serum globulins, which is not
370 known in zebrafish embryos (Miguel-Queralt et al., 2004).

371 We also calculated the percent uptake of testosterone per embryo. We found that
372 the percent uptake was 0.22% ± 0.11% per embryo (mean ± SD, Fig. 3). The low
373 uptake from water is consistent with our previous results for the structurally similar
374 steroid, 17β-estradiol, where we found that 1% or less of estradiol in fish water is taken
375 up into embryos, depending on embryo stage (Souder and Gorelick, 2017). Note that we
376 were unable to detect testosterone in untreated embryos. We conclude that
377 endogenous testosterone levels at these stages of embryonic development are below
378 the limit of detection, at least when pooling 50 embryos. Taken together, our results
379 suggest that only a small percentage of testosterone in the water is absorbed by the
380 embryo, and that supra-physiologic concentrations of testosterone in the fish water are
381 justified because it results in close to human physiologic levels in embryos.

382

383 **Testosterone, but not androstanedione or DHT, act via GPRC6A to cause cardiac**
384 **edema**

385 In the experiments described above, we showed that nuclear *ar* mutant embryos
386 remained sensitive to androstanedione, DHT, or testosterone exposure, suggesting the
387 involvement of *ar*-independent pathways. To determine whether these androgens act
388 via putative membrane androgen receptors, we took an F0 CRISPR genome editing
389 approach to generate zebrafish with mosaic mutations in putative membrane androgen

390 receptor genes: *gprc6a*, *zip9*, *oxer1* (*hcar1-4), cacna1c* (*cav1.2*) (Thomas, 2019;
391 Treviño and Gorelick, 2021)(Fig. S2). This approach enables us to inject embryos with a
392 cocktail of 4 guide RNAs together with Cas9 protein, targeting the same gene
393 redundantly, which induces mutations at a high enough burden to observe phenotypes
394 in the injected embryos (Hoshijima et al., 2019; Kroll et al., 2021; Wu et al., 2018).
395 We exposed embryos injected with gRNAs targeting *gprc6a*, *zip9*, *hcar1-4,*
396 *cacna1c*, or control embryos injected with Cas9 alone, to androstanedione, DHT,
397 testosterone or vehicle (0.1% DMSO) beginning at 3 hours post fertilization and
398 assayed morphology at 2- and 3-days post fertilization. Following androstanedione,
399 DHT, or testosterone exposure, *hcar1-4* and *zip9* mutant embryos exhibited cardiac
400 edema or tail curvature phenotype (Fig. 4). Untreated *cacna1c* mosaic mutant embryos
401 exhibited cardiac edema with abnormal heart morphology at 3 days post fertilization (not
402 shown). Therefore, we excluded *cacna1c* from further screening. Following chemical
403 exposure, we found no statistically significant difference in the proportion of embryos
404 with cardiac edema or tail curvature phenotype between control or *hcar1-4* and *zip9* F0
405 mosaic mutants (Fig 4, Table 2).
406 We found that *gprc6a* mosaic mutants had a statistically significant reduction in
407 the percent of embryos exhibiting cardiac edema following testosterone exposure (Fig.
408 4B, Table 3; embryos injected with Cas9 alone mean cardiac edema 65% ± 11%,
409 *gprc6a* mosaic mutants 45% ± 9%, n=8 clutches, 42-164 embryos per clutch). However,
410 the *gprc6a* mosaic mutants remained sensitive to androstanedione or DHT exposure
411 (Fig. 4B, Table 2). As an additional control, we injected wild-type embryos with Cas9
412 plus gRNAs targeting an unrelated gene encoding an aryl hydrocarbon receptor *(ahr2)*.

413 We exposed *ahr2* mosaic mutant embryos to testosterone and assayed cardiac edema
414 phenotype at 3 days post fertilization. There was no statistically significant difference in
415 the percent embryos exhibiting cardiac edema between control embryos versus *ahr2*
416 mosaic mutant embryos (Fig. 4C, Table 2). We conclude that the testosterone exposure
417 phenotype is partially rescued by mutating *gprc6a*.

418 To test whether there is crosstalk between GPRC6A and the canonical nuclear
419 androgen receptor *ar* (also known as *nr3c4*), we generated mosaic double mutant
420 embryos by injecting 1-cell stage $ar^{uab142/uab142}$ embryos with a cocktail of 4 guide RNAs
421 targeting the *gprc6a* gene (the same gRNAs used above). We exposed double mutant
422 embryos to testosterone (30 μM) to test whether the phenotype is the same as in single
423 mutant embryos. There was no statistically significant difference in the percent embryos
424 exhibiting cardiac edema between *gprc6a* mosaic mutants on wild-type background
425 versus *gprc6a* mosaic mutants on $ar^{uab142/uab142}$ mutant background (Fig. 5). We
426 conclude that testosterone acts through *gprc6a* independently of nuclear *ar.* This is
427 consistent with results from cultured cells and adult mouse tissues suggesting that
428 GPRC6A responds to testosterone (Pi et al., 2010; Pi et al., 2015).

429

430 **CRISPR–Cas9 mutagenesis efficiency in F0 embryos**

431 The absence of a phenotype in a CRISPR screen could be due to low efficiency of
432 gRNAs. It is possible that targeting *zip9* or *hcar1-4* failed to rescue androgen
433 phenotypes because the *zip9* and *hcar1-4* gRNAs had low efficacy. To evaluate the
434 mutagenesis efficiency in our F0 embryos, we isolated genomic DNA from individual
435 embryos at 24 hours post fertilization. The targeted site was amplified using PCR.

436 Amplicons were Sanger sequenced and then deconvoluted and analyzed using the ICE
437 (Inference of CRISPR Edits) algorithm (Conant et al., 2022). We compared indel
438 mutations (the percent of sequence from each embryo that has a mutation) or knockout
439 score (the percent of mutations from each embryo that were predicted to produce a
440 non-functional protein) for each gRNA (Fig. S3). Different guides acted with variable
441 effectiveness. In the cocktail of 4 guide RNA sets to target *gprc6a*, G4 produced an
442 average of more than 50% indel mutations or knockout score (n=38 embryos from 2
443 clutches). G1 and G2 were less effective, with an average mutation frequency of less
444 than 10% (n=40 embryos from 2 clutches), and G3 produced 0% mutation (n=38
445 embryos from 2 clutches) (Fig. S3).
446 Comparing the efficiency of guide RNAs targeting *zip9*, G1, and G3 were the
447 most effective. G1 induced an average of 78% indel mutations (n=40 embryos from 2
448 clutches) or 52% knockout score (n=40 embryos from 2 clutches), and G3 induced an
449 average of 73% indel mutations (n=45 embryos from 2 clutches) or 5% knockout score
450 (n=45 embryos from 2 clutches). For *hcar1-4*, the average indel mutations or knockout
451 score for all G1, G2, and G4 was greater than 50% (n=2 clutches/24-45 embryos per
452 clutch). In analyzed *hcar1-4* mosaic mutant embryos, G4 induced greater than 90%
453 indel mutations or knockout-score (n=46 embryos from 2 clutches). Overall, these
454 results confirm the efficacy of multi-locus targeting to generate zebrafish F0 mutants for
455 the purpose of initial screening of gene function.
456
457 **Zygotic *gprc6a* mutants recapitulate phenotypes observed in mosaic mutants**

458 To validate our observations, we generated heritable, non-mosaic mutations in
459 *gprc6a* and determined whether homozygous embryos were protected from
460 testosterone-dependent cardiac edema, as were F0 mosaic mutants. We injected wild-
461 type embryos with Cas9 together with the same set of 4 guide RNAs, targeting different
462 coding regions of the *gprc6a* gene, as we did to generate *gprc6a* mosaic mutants (Fig.
463 S4). Injected embryos were raised to adulthood and outcrossed to wild-type zebrafish to
464 generate heterozygous F1 embryos. Heterozygous F1 adult fish were sequenced to
465 identify mutations predicted to cause loss of functional GPRC6A protein. We identified
466 several mutant alleles in F1 fish and derived five independent *gprc6a* mutant lines, from
467 which we performed experiments on homozygous embryos: *gprc6a* $^{bcm53/-;\ bcm52/-}$, *gprc6a*
468 $^{bcm56/-;\ bcm54/-;\ bcm55/-}$, *gprc6a* $^{bcm56/-;\ bcm54/-}$, *gprc6a* $^{bcm59/-;\ bcm58/-}$, and *gprc6a* $^{bcm61/-;\ bcm60/-}$
469 (Fig. S4A). For example, *bcm53* is a 1 bp deletion in exon 1 resulting in a frameshift at
470 amino acid 44 and a premature stop codon at amino acid 50 in the ligand binding
471 domain. *bcm5*2 is a 1 bp deletion in exon 3 resulting in a frameshift at amino acid 225
472 and a premature stop codon at amino acid 250. These two alleles are genetically linked
473 (we were unable to generate fish containing *bcm52* without *bcm53*), however the
474 upstream allele (*bcm53*) is likely driving the loss of function. We did not observe any
475 morphologic differences among untreated *gprc6a* $^{bcm53/-;\ bcm52/-}$, *gprc6a* $^{bcm56/-;\ bcm54/-;}$
476 $^{bcm55/-}$, *gprc6a* $^{bcm56/-;\ bcm54/-}$, *gprc6a* $^{bcm59/-;\ bcm58/-}$, and *gprc6a* $^{bcm61/-;\ bcm60/-}$ embryos.
477 We exposed homozygous *gprc6a* embryos to vehicle, androstanedione, DHT, or
478 testosterone beginning at 3 hours post fertilization. Each clutch contained a mix of wild-
479 type and mutant embryos (denoted as wild-type +/+, heterozygous +/-, or homozygous -
480 /-; Fig. 6A). Following testosterone exposure, homozygous *gprc6a* mutant embryos

481 exhibited partial cardiac edema rescue, similar to what we observed in mosaic F0
482 mutants (Figure 4B, Table 3; wild-type mean percent cardiac edema 76% ± 9%,
483 heterozygous 76% ± 8%, homozygous 58% ± 10%, n=13 clutches, 12-57 embryos per
484 clutch). Analyzing the response of each allele separately revealed similar results (Fig.
485 S5, Table 3). Homozygous *gprc6a* mutants remained sensitive to androstanedione and
486 DHT exposure, similar to wild-type embryos (Fig. 6B, Table 3). We conclude that the F0
487 CRISPR *gprc6a* mosaic mutants recapitulate what occurs in non-mosaic homozygous
488 mutants. Taken together, our results suggest that testosterone causes cardiac edema
489 by acting via the integral membrane protein GPRC6A independently of the nuclear *ar*.
490

491 **GPRC6A antagonists inhibit testosterone-dependent cardiac edema in wild-type**
492 **embryos**

493 To further confirm that testosterone acts through *gprc6a* to cause cardiac edema,
494 we tested whether GPRC6A antagonists block testosterone-driven cardiac edema. We
495 exposed wild-type embryos to testosterone together with different GPRC6A antagonists,
496 NPS-2143 (5 μM), calindol (5 μM), and epigallocatechin gallate (EGCG, 100 μM) at
497 concentrations used to study GPRC6A responses in cultured cells (Faure et al., 2009;
498 Mizuta et al., 2021; Pi et al., 2018). We confirmed that 5 μM NPS-2143, 5 μM calindol,
499 and 100 μM EGCG do not cause abnormalities in embryos in the absence of androgen
500 exposure (Fig. 7A, Table 4). We found that wild-type embryos exposed to NPS-2143 or
501 EGCG with testosterone had statistically significantly reduced cardiac edema compared
502 to embryos exposed to testosterone alone (Fig. 7A, Table 4; testosterone mean
503 embryos with cardiac edema 69% ± 7%, testosterone + NPS-2143 39% ± 9%,

504 testosterone + EGCG 32% ± 8%, n=6 clutches, 43-63 embryos per clutch). While NPS-
505 2143 and EGCG partially blocked testosterone-driven cardiac edema, calindol failed to
506 reduce testosterone-dependent cardiac edema (Fig. 7A, Table 4). Calindol was
507 developed as a calcimimetic that binds the human calcium sensing receptor and has
508 lower selectivity towards GPRC6A (Gloriam et al., 2011; Kessler et al., 2004). The
509 failure of calindol to inhibit zebrafish GPRC6A could be due to the lower selectivity
510 together with differences between zebrafish and human GPRC6A proteins.
511 To test whether NPS-2143 and EGCG act specifically on zebrafish GPRC6A, we
512 exposed homozygous *gprc6a* mutant embryos to testosterone alone or together with
513 NPS-2143 and EGCG and assayed cardiac edema. There was no statistically
514 significant difference in the percent of *gprc6a* homozygous embryos exhibiting cardiac
515 edema following exposure to NPS-2143 or EGCG alone or in combination with
516 testosterone (Fig. 7B, Table 4; testosterone mean embryos with cardiac edema 45% ±
517 5%, testosterone + NPS-2143 55% ± 5%, testosterone + EGCG 47% ± 6%, n=4
518 clutches, 18-30 embryos per clutch). These results show that the zebrafish *gprc6a*
519 mutants do not respond to GPRC6A antagonists and supports the hypothesis that
520 testosterone acts via GPRC6A to cause cardiac edema.
521
522 **Testosterone, and not a metabolite, causes cardiac edema in a GPRC6A-**
523 **dependent manner**
524 Testosterone is metabolized into molecules like estradiol. We showed that exposure to
525 testosterone caused cardiac edema in a GPRC6A-dependent manner. However, it is
526 not known whether testosterone, or a metabolite, is the active compound that causes

527 the phenotype. We hypothesize that testosterone itself acts on GPRC6A to cause
528 cardiac edema in zebrafish embryos. To test whether estradiol, a testosterone
529 metabolite, causes a phenotype similar to testosterone, we exposed wild-type embryos
530 at 3 hours post fertilization to 30 μM estradiol or 30 μM testosterone and assayed
531 morphologic phenotypes at 3 days post fertilization. We found that exposure of wild-type
532 embryos to estradiol did not cause cardiac edema or other morphologic phenotypes
533 (Fig. 8A, Table 5), supporting the hypothesis that testosterone, and not estradiol, is the
534 active compound that causes the phenotype.

535 To further test whether testosterone acts on GPRC6A directly *in vivo*, we
536 generated aromatase mutant embryos and asked whether testosterone causes a
537 phenotype in an aromatase-dependent manner. Aromatase is the rate-limiting enzyme
538 in the conversion of testosterone into estradiol (Conley and Hinshelwood, 2001; Duffy et
539 al., 2010). Zebrafish have two aromatase genes, *cyp19a1a* and *cyp19a1b* (Chiang et
540 al., 2001a; Chiang et al., 2001b). *cyp19a1a* is expressed exclusively in the gonads
541 (which do not begin developing until ~10 days post fertilization), while *cyp19a1b* is
542 expressed in the brain at 2 days post fertilization (Chiang et al., 2001a; Chiang et al.,
543 2001b; Lassiter and Linney, 2007). Here we focused on the *cyp19a1b* gene because of
544 its expression during embryonic development.

545 Using CRISPR/Cas9, we generated heritable mutant alleles for *cyp19a1b* with a
546 20 bp insertion in exon 2 (Fig. S6A, maternal zygotic *cyp19a1b* mutant *MZcyp19a1b*
547 ^{uab124}). The mutation is predicted to result in a frameshift at amino acid 11 and a
548 premature stop codon at amino acid 30 (Fig. S6B). We exposed *MZcyp19a1b* ^{uab124}
549 embryos to vehicle (0.1% DMSO) or testosterone at 3 hours post fertilization and

550 assayed morphologic phenotypes at 3 days post fertilization. *MZcyp19a1b* ^{uab124}
551 embryos remained sensitive to testosterone exposure, similar to what we observed
552 when wild-type embryos were exposed to testosterone (Fig. 8B, Table 5; wild-type
553 mean embryos cardiac edema 85% ± 8%, *MZcyp19a1b* 82% ± 6%, n=4 clutches, 21-35
554 embryos per clutch). These results suggest that aromatase is not required for
555 testosterone-dependent cardiac edema.
556 To exclude the possibility that testosterone acts via estrogen receptors (either via
557 non-specific binding or via crosstalk between GPRC6A and nuclear estrogen receptors),
558 we exposed estrogen receptor mutant embryos, *esr1a* $^{uab118/-}$ (ERα), *esr2a* $^{uab134/-}$
559 (ERβ1), and *esr2b* $^{uab128/-}$ (ERβ2) to testosterone. We found no significant difference in
560 the percent of embryos exhibiting cardiac edema phenotype between wild-type or
561 heterozygous embryos versus homozygous *esr1a* $^{uab118/-}$, *esr2a* $^{uab134/-}$, and *esr2b* $^{uab128/-}$
562 mutant embryos after testosterone exposure (Fig. 8C-E, Table 5). Taken together, these
563 results suggest that testosterone, and not a metabolite, is the active agent that causes
564 cardiac edema via GPRC6A.
565
566 **Genes regulated by T-GPRC6A**
567 To investigate the mechanisms by which testosterone causes heart defects via
568 GPRC6A, we performed RNA-sequencing (RNA-Seq) to identify genes regulated by T-
569 GPRC6A. By comparing genes expressed in wild-type embryos following exposure to
570 vehicle (0.1% DMSO), testosterone alone (30 μM), testosterone with EGCG (100 μM,
571 GPRC6A antagonist) or testosterone with calindol (5 μM, calcimimetic with GPRC6A
572 antagonism which was unable to rescue T-GPRC6A phenotype in Fig 7), we reasoned

573 we could identify genes specifically regulated by T-GPRC6A and distinguish these from
574 genes regulated by T-AR.
575 First, we generated 3 independent datasets from testosterone, calindol or EGCG
576 treatment over DMSO (dataset 1: testosterone over DMSO; dataset 2:
577 testosterone+calindol over DMSO; dataset 3: testosterone+EGCG over DMSO; Tables
578 S3, S4, and S5). Each dataset was generated by defining a differentially expressed
579 gene (DEG) as FDR < 0.05, irrespective of its fold change. We then made a list of T-
580 GPRC6A specific DEGs by combining the significant genes that are differentially
581 expressed in one direction (upregulated or downregulated in terms of fold change) in
582 both testosterone and testosterone+calindol treated groups but were rescued in the
583 testosterone +EGCG treated group by either showing no fold change or fold change in
584 the opposite direction (e.g. if genes are upregulated in testosterone, they will be
585 downregulated in testosterone+EGCG or vice versa, see Methods section for details).
586 Using these approaches, we identified 655 T-GPRC6A-specific DEGs (Table S6).
587 To identify and prioritize candidate genes, we focused on genes that were
588 downregulated by T-GPRC6A, reasoning that knockdown or mutation in these genes
589 should mimic the testosterone exposure phenotype, while overexpression of these
590 genes would rescue the testosterone exposure phenotype. We searched downregulated
591 genes against the ZFIN database (Bradford et al., 2022) to identify genes that are
592 expressed in the heart and genes for which a mutant or morpholino produced a cardiac
593 phenotype similar to what we observe following testosterone exposure. We identified 37
594 genes expressed in the heart (Table S7). Among these, 7 exhibited a cardiac

595 phenotype, of which 4 of them produced a phenotype similar to testosterone exposure
596 when knocked down or mutated (Table S7).
597
598 **Overexpression of *grk3* or *pak1* mRNA partially rescues the testosterone**
599 **exposure phenotype**
600 We initially focused on candidate gene *grk3*. GRK3 has been predominantly
601 recognized for its ability to desensitize GPCRs (Appleyard et al., 1999; Benovic et al.,
602 1991; Boekhoff et al., 1994; Diverse-Pierluissi et al., 1996; Terman et al., 2004). This is
603 achieved by phosphorylation of GPCR cytoplasmic domains and C termini that promote
604 interactions between the phosphorylated GPCRs and *β*-arrestins (Benovic et al., 1987;
605 Pitcher et al., 1992). This interaction sterically terminates G protein-mediated signaling.
606 Zebrafish *grk3* morphants exhibited a cardiac phenotype similar to testosterone
607 exposure (Jiang et al., 2009; Philipp et al., 2014). Thus, we would predict that
608 downregulating or mutating *grk3* would increase the ability of GPRC6A to respond to
609 testosterone, leading to cardiac abnormalities, while overexpressing *grk3* would reduce
610 the ability of GPRC6A to respond to testosterone (presumably by desensitizing
611 GPRC6A).
612 To test whether overexpression of *grk3* rescues the T-GPRC6A cardiac
613 phenotype, we injected wild-type, 1-cell stage embryos with *grk3* mRNA and exposed
614 them to testosterone or vehicle beginning at 3 hours post fertilization. We assayed
615 morphology 3 days post fertilization. We found that embryos overexpressing *grk3* had a
616 statistically significant reduction in cardiac edema following testosterone exposure
617 compared to negative control embryos injected with *gfp* mRNA or uninjected embryos

618 (Fig. 9; embryos injected with *grk3* mRNA mean cardiac edema 68% ± 4%, *gfp* mRNA
619 mean cardiac edema 94% ± 1%, and uninjected embryos mean cardiac edema 93% ±
620 3%, n=3-5 clutches, 29-71 embryos per clutch). These rescue results support the
621 hypothesis that testosterone acts via GPRC6A to cause cardiac phenotypes, while
622 desensitizing GPRC6A via GRK3 overexpression prevents testosterone from exerting
623 its deleterious effects on cardiac development (Fig. 10A).
624 We also focused on the candidate gene *pak1*. Zebrafish *pak1* knockdown
625 embryos displayed a cardiac defect similar to testosterone-treated embryos
626 (Jagadeeshan et al., 2017; Kelly et al., 2014; Lightcap et al., 2009). Whole-mount in situ
627 hybridization revealed expression of *pak1* in the heart at 48 hpf (Kelly et al., 2014). *pak1*
628 is a member of the serine/threonine kinase family, regulated by Ras-related GTPases
629 RAC1 and CDC42 (Manser et al., 1994). PAK1 functions through multiple downstream
630 proteins and signaling pathways, such as protein phosphatase 2A (Egom et al., 2016;
631 MacDougall et al., 1991), ion channels (Egom et al., 2016; Wang et al., 2014), cardiac
632 troponin I (Ke et al., 2004) and myosin light chain-2 (Monasky et al., 2012). In our RNA-
633 seq data, not only was *pak1* downregulated by T-GPRC6A (Table S6), but also several
634 ion channels involved in zebrafish cardiac function that are plausible PAK1 targets,
635 including *scn5Laa, itpr1b, kcnn3, kcnj14*, and *ftr01*, were downregulated by T-GPRC6A
636 (Table S6 and S7). Furthermore, a gene set enrichment analysis (GSEA) revealed
637 several ion transport/signaling pathways, consistent with PAK1 function, that were
638 downregulated in both the testosterone and testosterone+calindol treated groups and
639 rescued in the testosterone+EGCG treated group (Table S8, sodium ion
640 transmembrane transport, calcium-mediated signaling, calcium ion transmembrane

641 transport, cation transmembrane transport, among others). These findings encouraged
642 us to prioritize *pak1* as a candidate.
643 To test whether overexpression of *pak1* rescues the T-GPRC6A cardiac
644 phenotype, we injected wild-type, 1-cell stage embryos with *pak1* mRNA and exposed
645 them to testosterone or vehicle beginning at 3 hours post fertilization. We assayed
646 morphology 3 days post fertilization. Similar to overexpressing *grk3*, we found that
647 embryos overexpressing *pak1* also had a statistically significant reduction in cardiac
648 edema following testosterone exposure compared to negative control embryos injected
649 with *gfp* mRNA or uninjected embryos (Fig. 9; embryos injected with *pak1* mRNA mean
650 cardiac edema 66% ± 8%, *GFP* mRNA mean cardiac edema 94% ± 1%, and uninjected
651 embryos mean cardiac edema 93% ± 3%, n=3-5 clutches, 29-71 embryos per clutch).
652 We conclude that GPRC6A, when activated by testosterone, inhibits PAK1 activity,
653 leading to abnormal cardiac development (Fig. 10B, C).
654
655 **Discussion**
656 We demonstrate that a CRISPR screen in zebrafish embryos can be used to
657 identify genes required for testosterone-dependent phenotypes. The zebrafish
658 screening approach complements existing cell-based approaches. Membrane steroid
659 receptors are typically identified based on their binding or activity in cultured cells, and
660 then tested for similar activity *in vivo*. It can be difficult to determine whether a receptor
661 responds to steroids *in vivo*, especially receptors that have multiple ligands. For
662 example, the estrogen receptor modulator tamoxifen was shown to bind directly to the
663 human sodium channel Nav1.2 and inhibit sodium conductance *in vitro* (Sula et al.,

664 2021), but whether this occurs *in vivo* is not known. The zebrafish screening approach
665 allows for the direct identification of membrane steroid receptors *in vivo*.
666 Our approach relies on using CRISPR-Cas9 to rapidly generate mutant
667 zebrafish. To generate heritable mutants, germline transmitting animals need to be
668 identified and mated to produce homozygous embryos, a process that takes months. In
669 contrast, analyzing gene function in mosaic mutant animals (F0 generation) takes less
670 than a week. Our approach was enabled by recent findings that injecting zebrafish
671 embryos with Cas9 protein and a cocktail of 3-4 guide RNAs targeting the same gene
672 induces mutations at a high enough burden to observe phenotypes in mosaic mutant
673 embryos (Klatt Shaw and Mokalled, 2021; Kroll et al., 2021; Wu et al., 2018). One
674 potential limitation of CRISPR screens is the failure of F0 mosaic mutants to
675 recapitulate phenotypes found in heritable, non-mosaic mutants (eg F1 and subsequent
676 generations). In our screen, this was not the case. We identified similar phenotypes in
677 F0 mosaic and in non-mosaic *gprc6a* mutants (compare Figures 4 and 6),
678 demonstrating the validity of using the F0 CRISPR screening approach.
679 Our pilot screen tested 4 candidate genes using CRISPR-Cas9. However, new
680 barcoding and microfluidics approaches, such as MIC-Drop, could allow us to screen
681 and mutate hundreds or thousands of genes (Parvez et al., 2021). Combining different
682 chemical exposures with MIC-Drop offers the unprecedented ability to comprehensively
683 identify membrane receptors for any steroid molecule that causes a phenotype in
684 zebrafish embryos. Here, we assayed gross, easily observable morphologic
685 phenotypes. It is also possible to assay more subtle phenotypes, for example by using

686 transgenic reporter zebrafish that mark a cell-type of interest, or by using assays to
687 measure behaviors like locomotor activity.

688 We found that testosterone exposure caused cardiac edema and heart
689 malformations in approximately 80% of wild-type embryos. This phenotype was partially
690 rescued by co-administration of two different GPRC6A antagonists (Figure 7). The
691 testosterone phenotype was also partially rescued in *gprc6a* mutants (both mosaic F0
692 and heritable homozygotes, Figure 4, Figure 6). Similar results using F0 mosaic
693 mutants, F0 non-mosaic mutants, and pharmacologic antagonists, plus rescue with
694 overexpression of *grk3* and *pak1* (Figure 9), suggests the partial rescue is not an artifact
695 of mutagenesis. What explains the lack of a complete rescue? Testosterone could also
696 be acting simultaneously through multiple pathways, for example by binding to
697 additional receptors or by altering the fluidity of cell membranes or the mobility of
698 membrane proteins (Liang et al., 2001; Shivaji and Jagannadham, 1992; Whiting et al.,
699 1995; Whiting et al., 2000). The fact that the testosterone phenotype in *gprc6a;ar* double
700 mutants was similar to *gprc6a* single mutants (Figure 5) suggests that T-GPRC6A acts
701 independently of AR in this case.

702 Our results are the first to identify a role for androgen-dependent GPRC6A
703 activity during embryonic development. Our results are consistent with results from
704 cultured cells and mouse models demonstrating that GPRC6A responds to
705 testosterone. In HEK-293 cells, testosterone stimulated extracellular signal-regulated
706 kinase (ERK) activity, which was blocked by GPRC6A antagonists (Pi et al., 2018). In
707 wild-type mice, testosterone treatment increased levels of phosphorylated ERK and
708 Egr-1 expression in bone marrow and testis, which was reduced or absent in GPRC6A

709 mutant mice (Pi et al., 2010). Several ligands activate GPRC6A, including calcium,
710 magnesium, and the peptide hormone osteocalcin (Pi et al., 2005). It remains to be seen
711 whether or how testosterone influences the response of GPRC6A to other ligands.
712 Osteocalcin is maternally deposited into zebrafish oocytes and expressed at 2 days
713 post fertilization (Bensimon-Brito et al., 2012), developmental stages when embryos
714 exposed to testosterone exhibit cardiac phenotypes. Future studies could explore
715 whether osteocalcin is required for testosterone-GPRC6A-dependent cardiac
716 phenotypes.

717 We also discovered part of the mechanism by which T-GPRC6A regulates
718 cardiac development, via the serine/threonine kinase PAK1. Overexpression of *pak1*
719 partially rescued the testosterone exposure phenotype in wild-type embryos (Fig 9). A
720 previous report found that zebrafish pak1 signals through the Erk pathway and the
721 transcription factor Gata6 to promote proper heart development (Kelly et al., 2014). Our
722 results are consistent with this observation. We propose that exogenous testosterone
723 activates GPRC6A, which then inhibits Pak1 and leads to abnormal heart development
724 (Fig. 10). In the absence of testosterone, Pak1 is free to activate its downstream
725 targets, which may include Erk/Gata6 but could also include ion channels and
726 transporters required for normal heart development. Using RNA-seq, we identified
727 several ion channel genes downregulated by T-GPRC6A. While the interaction between
728 these ion channels and *pak1* has not been investigated in zebrafish, they could play a
729 role in cardiac development and function similar to ion channels known to function
730 downstream of Pak1 in other organisms.

731 Our ELISA results show that an average of ~60 nM testosterone per embryo
732 causes a phenotype. We failed to detect any testosterone in untreated embryos. We
733 hypothesize that under normal conditions, zebrafish embryos at 0-3 dpf contain low
734 levels of testosterone, which allow the heart to develop normally (Fig 10). Increasing
735 testosterone levels activates GPRC6A, which leads to improper heart development.
736 Because the zebrafish gonad does not differentiate until approximately 10 dpf, it is likely
737 that endogenous levels of testosterone are low until that time. It is possible that in
738 zebrafish, the heart (and other organs) are more sensitive to testosterone exposure
739 during early periods of differentiation and development. Once developed and more
740 mature, the heart may be less susceptible to potentially deleterious effects of
741 testosterone exposure. This idea of a critical window of sensitivity is consistent with data
742 from sheep. Pregnant ewes exposed to increased testosterone between gestational
743 days 30 and 59 produced fetuses with smaller hearts due to reduced cardiomyocyte
744 maturation and proliferation (fetuses were delivered at 135 days). In contrast, pregnant
745 ewes exposed to increased testosterone between gestation days 60 and 90 had normal
746 cardiac growth and development (Jonker et al., 2018).
747 Gestational testosterone excess, such as occurs in polycystic ovarian syndrome
748 (Sir-Petermann et al., 2002), is associated with fetal abnormalities that increase risks for
749 heart dysfunction later in life. Fetal sheep exposed to increased testosterone exhibited
750 myocardial disarray in the left ventricle, increased cardiomyocyte size, increased
751 expression of genes associated with cardiac hypertrophy, and fetal growth retardation
752 (Ghnenis et al., 2022; Manikkam et al., 2004; Ramamoorthi Elangovan et al., 2023; Vyas
753 et al., 2016). In rats, maternal testosterone excess was associated with cardiac

754 hypertrophy in offspring (Hou et al., 2019). While the molecular mechanisms of how
755 testosterone causes these phenotypes is not well understood, the assumption is that
756 these phenotypes are caused by testosterone activating canonical nuclear androgen
757 receptors. Our results in zebrafish suggest that gestational testosterone excess may
758 also cause deleterious effects via membrane androgen receptors like GPRC6A.
759 Furthermore, studying the effects of excess androgens in zebrafish embryos could
760 provide insights into how gestational hyperandrogenism associated with polycystic
761 ovarian syndrome affects fetal development.

762 Our chemical-genetic F0 CRISPR screening approach has several limitations.
763 Our scheme relies on identifying phenotypes following exposure to steroids, and then
764 testing whether a gene mutation rescues the exposure phenotype (Figure 1). If a mutant
765 has a phenotype in the absence of chemical exposure, then we cannot test that gene.
766 For example, embryos injected with gRNAs targeting *cav1.2* exhibited cardiac edema in
767 the absence of chemical exposure. Consequently, we could not test whether *cav1.2*
768 mutations rescue testosterone-dependent cardiac edema. This also demonstrates the
769 strength of the approach. The phenotype we observed in *cav1.2* mosaic mutants was
770 similar to the phenotypes observed in *cav1.2* heritable, homozygous mutants (Rottbauer
771 et al., 2001), further supporting the idea that F0 mosaic mutants recapitulate
772 phenotypes observed in heritable, non-mosaic mutants.

773 Another limitation is that genetic compensation could produce false negative
774 results. A mutation in a gene could lead to upregulation of a related gene that
775 compensates for the original mutation. In this case, we would falsely conclude that the
776 target gene is not involved in steroid signaling. Future studies can overcome this

777 limitation by performing a deletion screen, using two gRNAs flanking the target gene to
778 delete the entire target gene. This would prevent production of mRNA and consequently
779 would reduce the occurrence of compensation triggered by mutant mRNA (El-Brolosy et
780 al., 2019; Fernandez-Abascal et al., 2022; Ma et al., 2019; Serobyan et al., 2020).
781 Another concern are phenotypes resulting from the off-target effects of Cas9. These can
782 be validated by performing RNA rescue studies or by generating heritable, non-mosaic
783 mutations in the target gene. By successively breeding such mutants with wild-type
784 animals, one selects for the target mutation and loses potential off-target mutations.
785 This is the strategy we employed. We found that homozygous *gprc6a* mutants are
786 partially resistant to testosterone exposure (Figure 6), similar to what we observed in
787 mosaic *gprc6a* F0 mutants (Figure 4). Thus, the off-target effects of Cas9 are unlikely to
788 influence our results.
789 In conclusion, we developed a combined chemical and genetic screening
790 approach to identify genes required for androgen-dependent phenotypes in zebrafish
791 embryos. Our pilot screen revealed that testosterone acts via GPRC6A to cause cardiac
792 phenotypes. This chemical-genetic screening platform can be adapted to discover
793 genes encoding membrane proteins that act as receptors for any steroid or related
794 small molecule.
795

796 **Acknowledgements**

797 We thank Lauren Pandolfo and the staff of the BCM zebrafish facility for caring for our
798 zebrafish, the members of NR IMPACT for scientific feedback during the early phases
799 of this project, and members of the Gorelick laboratory for advice on experiments. This

800 work was supported by the NIH Training Program in Precision Environmental Health
801 Sciences T32 ES027801. The Baylor College of Medicine high-performance computing
802 cluster, managed by the Biostatistics and Informatics Shared Resource, is supported by
803 grants from NCI P30-CA125123 and Institutional funds from the Dan L Duncan
804 Comprehensive Cancer Center and Baylor College of Medicine. Figures 1 and 10 were
805 created using Biorender.com.
806

807 **References**

808

809 **Appleyard, S. M., Celver, J., Pineda, V., Kovoor, A., Wayman, G. A. and Chavkin,**
810 **C.** (1999). Agonist-dependent desensitization of the kappa opioid receptor by G
811 protein receptor kinase and beta-arrestin. *J. Biol. Chem.* **274**, 23802–23807.

812 **Asuthkar, S., Elustondo, P. A., Demirkhanyan, L., Sun, X., Baskaran, P., Velpula,**
813 **K. K., Thyagarajan, B., Pavlov, E. V. and Zakharian, E.** (2015a). The TRPM8
814 protein is a testosterone receptor: I. Biochemical evidence for direct TRPM8-
815 testosterone interactions. *J. Biol. Chem.* **290**, 2659–2669.

816 **Asuthkar, S., Demirkhanyan, L., Sun, X., Elustondo, P. A., Krishnan, V., Baskaran,**
817 **P., Velpula, K. K., Thyagarajan, B., Pavlov, E. V. and Zakharian, E.** (2015b). The
818 TRPM8 protein is a testosterone receptor: II. Functional evidence for an ionotropic
819 effect of testosterone on TRPM8. *J. Biol. Chem.* **290**, 2670–2688.

820 **Bakker, J.** (2022). The role of steroid hormones in the sexual differentiation of the
821 human brain. *J. Neuroendocrinol.* **34**, e13050.

822 **Benovic, J. L., Kühn, H., Weyand, I., Codina, J., Caron, M. G. and Lefkowitz, R. J.**
823 (1987). Functional desensitization of the isolated beta-adrenergic receptor by the
824 beta-adrenergic receptor kinase: potential role of an analog of the retinal protein
825 arrestin (48-kDa protein). *Proc Natl Acad Sci USA* **84**, 8879–8882.

826 **Benovic, J. L., Onorato, J. J., Arriza, J. L., Stone, W. C., Lohse, M., Jenkins, N. A.,**
827 **Gilbert, D. J., Copeland, N. G., Caron, M. G. and Lefkowitz, R. J.** (1991). Cloning,
828 expression, and chromosomal localization of beta-adrenergic receptor kinase 2. A
829 new member of the receptor kinase family. *J. Biol. Chem.* **266**, 14939–14946.

830 **Bensimon-Brito, A., Cardeira, J., Cancela, M. L., Huysseune, A. and Witten, P. E.**
831 (2012). Distinct patterns of notochord mineralization in zebrafish coincide with the
832 localization of Osteocalcin isoform 1 during early vertebral centra formation. *BMC*
833 *Dev. Biol.* **12**, 28.

834 **Benten, W. P., Lieberherr, M., Stamm, O., Wrehlke, C., Guo, Z. and Wunderlich, F.**
835 (1999). Testosterone signaling through internalizable surface receptors in androgen
836 receptor-free macrophages. *Mol. Biol. Cell* **10**, 3113–3123.

837 **Boekhoff, I., Inglese, J., Schleicher, S., Koch, W. J., Lefkowitz, R. J. and Breer, H.**
838 (1994). Olfactory desensitization requires membrane targeting of receptor kinase
839 mediated by beta gamma-subunits of heterotrimeric G proteins. *J. Biol. Chem.* **269**,
840 37–40.

841 **Bradford, Y. M., Van Slyke, C. E., Ruzicka, L., Singer, A., Eagle, A., Fashena, D.,**
842 **Howe, D. G., Frazer, K., Martin, R., Paddock, H., et al.** (2022). Zebrafish
843 information network, the knowledgebase for Danio rerio research. *Genetics* **220**,.

844 **Burger, H. G.** (2002). Androgen production in women. *Fertil. Steril.* **77 Suppl 4**, S3-5.

845 **Burger, A., Lindsay, H., Felker, A., Hess, C., Anders, C., Chiavacci, E., Zaugg, J.,**
846 **Weber, L. M., Catena, R., Jinek, M., et al.** (2016). Maximizing mutagenesis with
847 solubilized CRISPR-Cas9 ribonucleoprotein complexes. *Development* **143**, 2025–
848 2037.

849 **Chang, C. S., Kokontis, J. and Liao, S. T.** (1988). Molecular cloning of human and rat
850 complementary DNA encoding androgen receptors. *Science* **240**, 324–326.

851 **Chiang, E. F., Yan, Y. L., Guiguen, Y., Postlethwait, J. and Chung Bc** (2001a). Two
852 Cyp19 (P450 aromatase) genes on duplicated zebrafish chromosomes are expressed
853 in ovary or brain. *Mol. Biol. Evol.* **18**, 542–550.

854 **Chiang, E. F., Yan, Y. L., Tong, S. K., Hsiao, P. H., Guiguen, Y., Postlethwait, J. and**
855 **Chung, B. C.** (2001b). Characterization of duplicated zebrafish cyp19 genes. *J. Exp.*
856 *Zool.* **290**, 709–714.

857 **Conant, D., Hsiau, T., Rossi, N., Oki, J., Maures, T., Waite, K., Yang, J., Joshi, S.,**
858 **Kelso, R., Holden, K., et al.** (2022). Inference of CRISPR Edits from Sanger Trace
859 Data. *The CRISPR Journal* **5**, 123–130.

860 **Conley, A. and Hinshelwood, M.** (2001). Mammalian aromatases. *Reproduction* **121**,
861 685–695.

862 **Converse, A. and Thomas, P.** (2020). The zinc transporter ZIP9 (Slc39a9) regulates
863 zinc dynamics essential to egg activation in zebrafish. *Sci. Rep.* **10**, 15673.

864 **Crowder, C. M., Lassiter, C. S. and Gorelick, D. A.** (2018). Nuclear androgen receptor
865 regulates testes organization and oocyte maturation in zebrafish. *Endocrinology* **159**,
866 980–993.

867 **Cunha, G. R., Kurita, T., Cao, M., Shen, J., Robboy, S. and Baskin, L.** (2017).
868 Molecular mechanisms of development of the human fetal female reproductive tract.
869 *Differentiation.* **97**, 54–72.

870 **Diverse-Pierluissi, M., Inglese, J., Stoffel, R. H., Lefkowitz, R. J. and Dunlap, K.**
871 (1996). G protein-coupled receptor kinase mediates desensitization of
872 norepinephrine-induced Ca2+ channel inhibition. *Neuron* **16**, 579–585.

873 **Dobin, A., Davis, C. A., Schlesinger, F., Drenkow, J., Zaleski, C., Jha, S., Batut, P.,**
874 **Chaisson, M. and Gingeras, T. R.** (2013). STAR: ultrafast universal RNA-seq
875 aligner. *Bioinformatics* **29**, 15–21.

876 **Duffy, T. A., Picha, M. E., Won, E. T., Borski, R. J., McElroy, A. E. and Conover, D.**
877 **O.** (2010). Ontogenesis of gonadal aromatase gene expression in atlantic silverside
878 (Menidia menidia) populations with genetic and temperature-dependent sex
879 determination. *J. Exp. Zool. A Ecol. Genet. Physiol.* **313**, 421–431.

880 **Egom, E. E.-A., Bae, J. S. H., Capel, R., Richards, M., Ke, Y., Pharithi, R. B., Maher,**
881 **V., Kruzliak, P. and Lei, M.** (2016). Effect of sphingosine-1-phosphate on L-type
882 calcium current and Ca(2+) transient in rat ventricular myocytes. *Mol. Cell. Biochem.*
883 **419**, 83–92.

884 **El-Brolosy, M. A., Kontarakis, Z., Rossi, A., Kuenne, C., Günther, S., Fukuda, N.,**
885 **Kikhi, K., Boezio, G. L. M., Takacs, C. M., Lai, S.-L., et al.** (2019). Genetic
886 compensation triggered by mutant mRNA degradation. *Nature* **568**, 193–197.

887 **Estrada, M., Liberona, J. L., Miranda, M. and Jaimovich, E.** (2000). Aldosterone- and
888 testosterone-mediated intracellular calcium response in skeletal muscle cell cultures.
889 *Am. J. Physiol. Endocrinol. Metab.* **279**, E132-9.

890 **Estrada, M., Espinosa, A., Müller, M. and Jaimovich, E.** (2003). Testosterone
891 stimulates intracellular calcium release and mitogen-activated protein kinases via a G
892 protein-coupled receptor in skeletal muscle cells. *Endocrinology* **144**, 3586–3597.

893 **Faure, H., Gorojankina, T., Rice, N., Dauban, P., Dodd, R. H., Bräuner-Osborne, H.,**
894 **Rognan, D. and Ruat, M.** (2009). Molecular determinants of non-competitive
895 antagonist binding to the mouse GPRC6A receptor. *Cell Calcium* **46**, 323–332.

896 **Fernandez-Abascal, J., Wang, L., Graziano, B., Johnson, C. K. and Bianchi, L.**
897 (2022). Exon-dependent transcriptional adaptation by exon-junction complex proteins
898 Y14/RNP-4 and MAGOH/MAG-1 in Caenorhabditis elegans. *PLoS Genet.* **18**,
899 e1010488.

900 **Finkelstein, J. S., Lee, H., Burnett-Bowie, S.-A. M., Pallais, J. C., Yu, E. W., Borges,**
901 **L. F., Jones, B. F., Barry, C. V., Wulczyn, K. E., Thomas, B. J., et al.** (2013).
902 Gonadal steroids and body composition, strength, and sexual function in men. *N.*
903 *Engl. J. Med.* **369**, 1011–1022.

904 **Fu, Y., Westenbroek, R. E., Yu, F. H., Clark, J. P., Marshall, M. R., Scheuer, T. and**
905 **Catterall, W. A.** (2011). Deletion of the distal C terminus of CaV1.2 channels leads to
906 loss of beta-adrenergic regulation and heart failure in vivo. *J. Biol. Chem.* **286**,
907 12617–12626.

908 **Gatson, J. W. and Singh, M.** (2007). Activation of a membrane-associated androgen
909 receptor promotes cell death in primary cortical astrocytes. *Endocrinology* **148**, 2458–
910 2464.

911 **Gatson, J. W., Kaur, P. and Singh, M.** (2006). Dihydrotestosterone differentially
912 modulates the mitogen-activated protein kinase and the phosphoinositide 3-
913 kinase/Akt pathways through the nuclear and novel membrane androgen receptor in
914 C6 cells. *Endocrinology* **147**, 2028–2034.

915 **Ghnenis, A., Padmanabhan, V. and Vyas, A.** (2022). Sexual dimorphism in
916 testosterone programming of cardiomyocyte development in sheep. *Am. J. Physiol.*
917 *Heart Circ. Physiol.* **322**, H607–H621.

918 **Gloriam, D. E., Wellendorph, P., Johansen, L. D., Thomsen, A. R. B., Phonekeo, K.,**
919 **Pedersen, D. S. and Bräuner-Osborne, H.** (2011). Chemogenomic discovery of
920 allosteric antagonists at the GPRC6A receptor. *Chem. Biol.* **18**, 1489–1498.

921 **Gorczynska, E. and Handelsman, D. J.** (1995). Androgens rapidly increase the
922 cytosolic calcium concentration in Sertoli cells. *Endocrinology* **136**, 2052–2059.

923 **Guo, Z., Benten, W. P. M., Krücken, J. and Wunderlich, F.** (2002). Nongenomic
924 testosterone calcium signaling. Genotropic actions in androgen receptor-free
925 macrophages. *J. Biol. Chem.* **277**, 29600–29607.

926 **Hatzoglou, A., Kampa, M., Kogia, C., Charalampopoulos, I., Theodoropoulos, P.**
927 **A., Anezinis, P., Dambaki, C., Papakonstanti, E. A., Stathopoulos, E. N.,**
928 **Stournaras, C., et al.** (2005). Membrane androgen receptor activation induces
929 apoptotic regression of human prostate cancer cells in vitro and in vivo. *J. Clin.*
930 *Endocrinol. Metab.* **90**, 893–903.

931 **Hoshijima, K., Jurynec, M. J., Klatt Shaw, D., Jacobi, A. M., Behlke, M. A. and**
932 **Grunwald, D. J.** (2019). Highly Efficient CRISPR-Cas9-Based Methods for
933 Generating Deletion Mutations and F0 Embryos that Lack Gene Function in
934 Zebrafish. *Dev. Cell* **51**, 645-657.e4.

935 **Hou, M., Gu, H.-C., Wang, H.-H., Liu, X.-M., Zhou, C.-L., Yang, Q., Jiang, Z.-R., Lin,**
936 **J., Wu, Y.-M., Wu, Y.-T., et al.** (2019). Prenatal exposure to testosterone induces
937 cardiac hypertrophy in adult female rats through enhanced Pkcδ expression in
938 cardiac myocytes. *J. Mol. Cell. Cardiol.* **128**, 1–10.

939 **Huang, C.-J., Tu, C.-T., Hsiao, C.-D., Hsieh, F.-J. and Tsai, H.-J.** (2003). Germ-line
940 transmission of a myocardium-specific GFP transgene reveals critical regulatory
941 elements in the cardiac myosin light chain 2 promoter of zebrafish. *Dev. Dyn.* **228**,
942 30–40.

943 **Jagadeeshan, S., Sagayaraj, R. V., Paneerselvan, N., Ghouse, S. S. and Malathi, R.**
944 (2017). Toxicity and anti-angiogenicity evaluation of Pak1 inhibitor IPA-3 using
945 zebrafish embryo model. *Cell Biol. Toxicol.* **33**, 41–56.

946 **Jao, L.-E., Wente, S. R. and Chen, W.** (2013). Efficient multiplex biallelic zebrafish
947 genome editing using a CRISPR nuclease system. *Proc Natl Acad Sci USA* **110**,
948 13904–13909.

949 **Jiang, X., Yang, P. and Ma, L.** (2009). Kinase activity-independent regulation of cyclin
950 pathway by GRK2 is essential for zebrafish early development. *Proc Natl Acad Sci*
951 *USA* **106**, 10183–10188.

952 **Jonker, S. S., Louey, S. and Roselli, C. E.** (2018). Cardiac myocyte proliferation and
953 maturation near term is inhibited by early gestation maternal testosterone exposure.
954 *Am. J. Physiol. Heart Circ. Physiol.* **315**, H1393–H1401.

955 **Jørgensen, A., Andersen, O., Bjerregaard, P. and Rasmussen, L. J.** (2007).
956 Identification and characterisation of an androgen receptor from zebrafish Danio rerio.
957 *Comp Biochem Physiol C Toxicol Pharmacol* **146**, 561–568.

958 **Kalyvianaki, K., Gebhart, V., Peroulis, N., Panagiotopoulou, C., Kiagiadaki, F.,**
959 **Pediaditakis, I., Aivaliotis, M., Moustou, E., Tzardi, M., Notas, G., et al.** (2017).
960 Antagonizing effects of membrane-acting androgens on the eicosanoid receptor
961 OXER1 in prostate cancer. *Sci. Rep.* **7**, 44418.

962 **Kang, H.-Y., Cho, C.-L., Huang, K.-L., Wang, J.-C., Hu, Y.-C., Lin, H.-K., Chang, C.**
963 **and Huang, K.-E.** (2004). Nongenomic androgen activation of phosphatidylinositol 3-
964 kinase/Akt signaling pathway in MC3T3-E1 osteoblasts. *J. Bone Miner. Res.* **19**,
965 1181–1190.

966 **Kelly, M. L., Astsaturov, A., Rhodes, J. and Chernoff, J.** (2014). A Pak1/Erk
967 signaling module acts through Gata6 to regulate cardiovascular development in
968 zebrafish. *Dev. Cell* **29**, 350–359.

969 **Kelsey, T. W., Li, L. Q., Mitchell, R. T., Whelan, A., Anderson, R. A. and Wallace, W.**
970 **H. B.** (2014). A validated age-related normative model for male total testosterone
971 shows increasing variance but no decline after age 40 years. *PLoS ONE* **9**, e109346.

972 **Kessler, A., Faure, H., Petrel, C., Ruat, M., Dauban, P. and Dodd, R. H.** (2004). N2-
973 benzyl-N1-(1-(1-naphthyl)ethyl)-3-phenylpropane-1,2-diamines and conformationally
974 restrained indole analogues: development of calindol as a new calcimimetic acting at
975 the calcium sensing receptor. *Bioorg. Med. Chem. Lett.* **14**, 3345–3349.

976 **Ke, Y., Wang, L., Pyle, W. G., de Tombe, P. P. and Solaro, R. J.** (2004). Intracellular
977 localization and functional effects of P21-activated kinase-1 (Pak1) in cardiac
978 myocytes. *Circ. Res.* **94**, 194–200.

979 **Klatt Shaw, D. and Mokalled, M. H.** (2021). Efficient CRISPR/Cas9 mutagenesis for
980 neurobehavioral screening in adult zebrafish. *G3 (Bethesda)* **11**,.

981 **Kroll, F., Powell, G. T., Ghosh, M., Gestri, G., Antinucci, P., Hearn, T. J., Tunbak,**
982 **H., Lim, S., Dennis, H. W., Fernandez, J. M., et al.** (2021). A simple and effective F0
983 knockout method for rapid screening of behaviour and other complex phenotypes.
984 *eLife* **10**,.

985 **Krueger, F.** (2015). Trim Galore!: A wrapper around Cutadapt and FastQC to
986 consistently apply adapter and quality trimming to FastQ files, with extra functionality
987 for RRBS data. *Babraham Institute*.

988 **Labun, K., Krause, M., Torres Cleuren, Y. and Valen, E.** (2021). CRISPR genome
989 editing made easy through the CHOPCHOP website. *Curr. Protoc.* **1**, e46.

990 **Lassiter, C. S. and Linney, E.** (2007). Embryonic expression and steroid regulation of
991 brain aromatase cyp19a1b in zebrafish (Danio rerio). *Zebrafish* **4**, 49–57.

992 **Liang, Y., Belford, S., Tang, F., Prokai, L., Simpkins, J. W. and Hughes, J. A.**
993 (2001). Membrane fluidity effects of estratrienes. *Brain Res. Bull.* **54**, 661–668.

994 **Liao, Y., Smyth, G. K. and Shi, W.** (2014). featureCounts: an efficient general purpose
995 program for assigning sequence reads to genomic features. *Bioinformatics* **30**, 923–
996 930.

997 **Lieberherr, M. and Grosse, B.** (1994). Androgens increase intracellular calcium
998 concentration and inositol 1,4,5-trisphosphate and diacylglycerol formation via a
999 pertussis toxin-sensitive G-protein. *J. Biol. Chem.* **269**, 7217–7223.

1000 **Lightcap, C. M., Kari, G., Arias-Romero, L. E., Chernoff, J., Rodeck, U. and**
1001 **Williams, J. C.** (2009). Interaction with LC8 is required for Pak1 nuclear import and is
1002 indispensable for zebrafish development. *PLoS ONE* **4**, e6025.

1003 **Liu, G., Honisch, S., Liu, G., Schmidt, S., Alkahtani, S., AlKahtane, A. A.,**
1004 **Stournaras, C. and Lang, F.** (2015). Up-regulation of Orai1 expression and store
1005 operated Ca(2+) entry following activation of membrane androgen receptors in MCF-7
1006 breast tumor cells. *BMC Cancer* **15**, 995.

1007 **Liu, G., Han, S., Jiang, S., Jiang, Y., Chen, C., Sun, N. and Che, H.** (2022).
1008 Extracellular Ca2+ aggravates IgE-induced allergic reaction in mast cells through
1009 GPRC6A, a novel family C G-protein-coupled receptor. *Life Sci.* **311**, 121013.

1010 **Lubahn, D. B., Joseph, D. R., Sullivan, P. M., Willard, H. F., French, F. S. and**
1011 **Wilson, E. M.** (1988a). Cloning of human androgen receptor complementary DNA
1012 and localization to the X chromosome. *Science* **240**, 327–330.

1013 **Lubahn, D. B., Joseph, D. R., Sar, M., Tan, J., Higgs, H. N., Larson, R. E., French,**
1014 **F. S. and Wilson, E. M.** (1988b). The human androgen receptor: complementary
1015 deoxyribonucleic acid cloning, sequence analysis and gene expression in prostate.
1016 *Mol. Endocrinol.* **2**, 1265–1275.

1017 **MacDougall, L. K., Jones, L. R. and Cohen, P.** (1991). Identification of the major
1018 protein phosphatases in mammalian cardiac muscle which dephosphorylate
1019 phospholamban. *Eur. J. Biochem.* **196**, 725–734.

1020 **Machelon, V., Nomé, F. and Tesarik, J.** (1998). Nongenomic effects of
1021 androstenedione on human granulosa luteinizing cells. *J. Clin. Endocrinol. Metab.* **83**,
1022 263–269.

1023 **Manikkam, M., Crespi, E. J., Doop, D. D., Herkimer, C., Lee, J. S., Yu, S., Brown, M.**
1024 **B., Foster, D. L. and Padmanabhan, V.** (2004). Fetal programming: prenatal
1025 testosterone excess leads to fetal growth retardation and postnatal catch-up growth in
1026 sheep. *Endocrinology* **145**, 790–798.

1027 **Manser, E., Leung, T., Salihuddin, H., Zhao, Z. S. and Lim, L.** (1994). A brain
1028 serine/threonine protein kinase activated by Cdc42 and Rac1. *Nature* **367**, 40–46.

1029 **Ma, Z., Zhu, P., Shi, H., Guo, L., Zhang, Q., Chen, Y., Chen, S., Zhang, Z., Peng, J.**
1030 **and Chen, J.** (2019). PTC-bearing mRNA elicits a genetic compensation response
1031 via Upf3a and COMPASS components. *Nature* **568**, 259–263.

1032 **Miguel-Queralt, S., Knowlton, M., Avvakumov, G. V., Al-Nouno, R., Kelly, G. M. and**
1033 **Hammond, G. L.** (2004). Molecular and functional characterization of sex hormone
1034 binding globulin in zebrafish. *Endocrinology* **145**, 5221–5230.

1035 **Mizuta, H., Kumamoto, N., Ugawa, S. and Yamamoto, T.** (2021). Additive Effects of
1036 L-Ornithine on Preferences to Basic Taste Solutions in Mice. *Nutrients* **13**,.

1037 **Mohr, B. A., Guay, A. T., O'Donnell, A. B. and McKinlay, J. B.** (2005). Normal, bound
1038 and nonbound testosterone levels in normally ageing men: results from the
1039 Massachusetts Male Ageing Study. *Clin Endocrinol (Oxf)* **62**, 64–73.

1040 **Monasky, M. M., Taglieri, D. M., Patel, B. G., Chernoff, J., Wolska, B. M., Ke, Y. and**
1041 **Solaro, R. J.** (2012). p21-activated kinase improves cardiac contractility during
1042 ischemia-reperfusion concomitant with changes in troponin-T and myosin light chain 2
1043 phosphorylation. *Am. J. Physiol. Heart Circ. Physiol.* **302**, H224-30.

1044 **Mootha, V. K., Lindgren, C. M., Eriksson, K.-F., Subramanian, A., Sihag, S., Lehar,**
1045 **J., Puigserver, P., Carlsson, E., Ridderstråle, M., Laurila, E., et al.** (2003). PGC-
1046 1alpha-responsive genes involved in oxidative phosphorylation are coordinately
1047 downregulated in human diabetes. *Nat. Genet.* **34**, 267–273.

1048 **Murashima, A., Kishigami, S., Thomson, A. and Yamada, G.** (2015). Androgens and
1049 mammalian male reproductive tract development. *Biochim. Biophys. Acta* **1849**, 163–
1050 170.

1051 **Parant, J. M., George, S. A., Pryor, R., Wittwer, C. T. and Yost, H. J.** (2009). A rapid
1052 and efficient method of genotyping zebrafish mutants. *Dev. Dyn.* **238**, 3168–3174.

1053 **Parvez, S., Herdman, C., Beerens, M., Chakraborti, K., Harmer, Z. P., Yeh, J.-R. J.,**
1054 **MacRae, C. A., Yost, H. J. and Peterson, R. T.** (2021). MIC-Drop: A platform for
1055 large-scale in vivo CRISPR screens. *Science* **373**, 1146–1151.

1056 **Philipp, M., Berger, I. M., Just, S. and Caron, M. G.** (2014). Overlapping and
1057 opposing functions of G protein-coupled receptor kinase 2 (GRK2) and GRK5 during
1058 heart development. *J. Biol. Chem.* **289**, 26119–26130.

1059 **Pitcher, J. A., Inglese, J., Higgins, J. B., Arriza, J. L., Casey, P. J., Kim, C.,**
1060 **Benovic, J. L., Kwatra, M. M., Caron, M. G. and Lefkowitz, R. J.** (1992). Role of
1061 beta gamma subunits of G proteins in targeting the beta-adrenergic receptor kinase to
1062 membrane-bound receptors. *Science* **257**, 1264–1267.

1063 **Pi, M. and Quarles, L. D.** (2012). GPRC6A regulates prostate cancer progression.
1064 *Prostate* **72**, 399–409.

1065 **Pi, M., Faber, P., Ekema, G., Jackson, P. D., Ting, A., Wang, N., Fontilla-Poole, M.,**
1066 **Mays, R. W., Brunden, K. R., Harrington, J. J., et al.** (2005). Identification of a
1067 novel extracellular cation-sensing G-protein-coupled receptor. *J. Biol. Chem.* **280**,
1068 40201–40209.

1069 **Pi, M., Chen, L., Huang, M.-Z., Zhu, W., Ringhofer, B., Luo, J., Christenson, L., Li,**
1070 **B., Zhang, J., Jackson, P. D., et al.** (2008). GPRC6A null mice exhibit osteopenia,
1071 feminization and metabolic syndrome. *PLoS ONE* **3**, e3858.

1072 **Pi, M., Parrill, A. L. and Quarles, L. D.** (2010). GPRC6A mediates the non-genomic
1073 effects of steroids. *J. Biol. Chem.* **285**, 39953–39964.

1074 **Pi, M., Kapoor, K., Wu, Y., Ye, R., Senogles, S. E., Nishimoto, S. K., Hwang, D.-J.,**
1075 **Miller, D. D., Narayanan, R., Smith, J. C., et al.** (2015). Structural and functional
1076 evidence for testosterone activation of GPRC6A in peripheral tissues. *Mol.*
1077 *Endocrinol.* **29**, 1759–1773.

1078 **Pi, M., Kapoor, K., Ye, R., Smith, J. C., Baudry, J. and Quarles, L. D.** (2018).
1079 GPCR6A is a molecular target for the natural products gallate and EGCG in green
1080 tea. *Mol. Nutr. Food Res.* **62**, e1700770.

1081 **Ramamoorthi Elangovan, V., Saadat, N., Ghnenis, A., Padmanabhan, V. and Vyas,**
1082 **A. K.** (2023). Developmental programming: adverse sexually dimorphic transcriptional

1083 programming of gestational testosterone excess in cardiac left ventricle of fetal
1084 sheep. *Sci. Rep.* **13**, 2682.

1085 **Risso, D., Ngai, J., Speed, T. P. and Dudoit, S.** (2014). Normalization of RNA-seq
1086 data using factor analysis of control genes or samples. *Nat. Biotechnol.* **32**, 896–902.

1087 **Robinson, M. D., McCarthy, D. J. and Smyth, G. K.** (2010). edgeR: a Bioconductor
1088 package for differential expression analysis of digital gene expression data.
1089 *Bioinformatics* **26**, 139–140.

1090 **Romano, S. N., Edwards, H. E., Souder, J. P., Ryan, K. J., Cui, X. and Gorelick, D.**
1091 **A.** (2017). G protein-coupled estrogen receptor regulates embryonic heart rate in
1092 zebrafish. *PLoS Genet.* **13**, e1007069.

1093 **Rosati, B., Yan, Q., Lee, M. S., Liou, S.-R., Ingalls, B., Foell, J., Kamp, T. J. and**
1094 **McKinnon, D.** (2011). Robust L-type calcium current expression following
1095 heterozygous knockout of the Cav1.2 gene in adult mouse heart. *J Physiol (Lond)*
1096 **589**, 3275–3288.

1097 **Rossetti, M. L., Steiner, J. L. and Gordon, B. S.** (2017). Androgen-mediated
1098 regulation of skeletal muscle protein balance. *Mol. Cell. Endocrinol.* **447**, 35–44.

1099 **Rottbauer, W., Baker, K., Wo, Z. G., Mohideen, M. A., Cantiello, H. F. and Fishman,**
1100 **M. C.** (2001). Growth and function of the embryonic heart depend upon the cardiac-
1101 specific L-type calcium channel alpha1 subunit. *Dev. Cell* **1**, 265–275.

1102 **Schindelin, J., Arganda-Carreras, I., Frise, E., Kaynig, V., Longair, M., Pietzsch, T.,**
1103 **Preibisch, S., Rueden, C., Saalfeld, S., Schmid, B., et al.** (2012). Fiji: an open-
1104 source platform for biological-image analysis. *Nat. Methods* **9**, 676–682.

1105 **Scragg, J. L., Jones, R. D., Channer, K. S., Jones, T. H. and Peers, C.** (2004).
1106 Testosterone is a potent inhibitor of L-type Ca(2+) channels. *Biochem. Biophys. Res.*
1107 *Commun.* **318**, 503–506.

1108 **Scragg, J. L., Dallas, M. L. and Peers, C.** (2007). Molecular requirements for L-type
1109 Ca2+ channel blockade by testosterone. *Cell Calcium* **42**, 11–15.

1110 **Seisenberger, C., Specht, V., Welling, A., Platzer, J., Pfeifer, A., Kühbandner, S.,**
1111 **Striessnig, J., Klugbauer, N., Feil, R. and Hofmann, F.** (2000). Functional
1112 embryonic cardiomyocytes after disruption of the L-type alpha1C (Cav1.2) calcium
1113 channel gene in the mouse. *J. Biol. Chem.* **275**, 39193–39199.

1114 **Serobyan, V., Kontarakis, Z., El-Brolosy, M. A., Welker, J. M., Tolstenkov, O.,**
1115 **Saadeldein, A. M., Retzer, N., Gottschalk, A., Wehman, A. M. and Stainier, D. Y.**
1116 (2020). Transcriptional adaptation in Caenorhabditis elegans. *eLife* **9**,.

1117 **Shivaji, S. and Jagannadham, M. V.** (1992). Steroid-induced perturbations of
1118 membranes and its relevance to sperm acrosome reaction. *Biochim. Biophys. Acta*
1119 **1108**, 99–109.

1120 **Sir-Petermann, T., Maliqueo, M., Angel, B., Lara, H. E., Pérez-Bravo, F. and**
1121 **Recabarren, S. E.** (2002). Maternal serum androgens in pregnant women with
1122 polycystic ovarian syndrome: possible implications in prenatal androgenization. *Hum.*
1123 *Reprod.* **17**, 2573–2579.

1124 **Souder, J. P. and Gorelick, D. A.** (2017). Quantification of estradiol uptake in zebrafish
1125 embryos and larvae. *Toxicol. Sci.* **158**, 465–474.

1126 **Subramanian, A., Tamayo, P., Mootha, V. K., Mukherjee, S., Ebert, B. L., Gillette,**
1127 **M. A., Paulovich, A., Pomeroy, S. L., Golub, T. R., Lander, E. S., et al.** (2005).
1128 Gene set enrichment analysis: a knowledge-based approach for interpreting genome-
1129 wide expression profiles. *Proc Natl Acad Sci USA* **102**, 15545–15550.

1130 **Sula, A., Hollingworth, D., Ng, L. C. T., Larmore, M., DeCaen, P. G. and Wallace, B.**
1131 **A.** (2021). A tamoxifen receptor within a voltage-gated sodium channel. *Mol. Cell* **81**,
1132 1160-1169.e5.

1133 **Sun, Y.-H., Gao, X., Tang, Y.-J., Xu, C.-L. and Wang, L.-H.** (2006). Androgens induce
1134 increases in intracellular calcium via a G protein-coupled receptor in LNCaP prostate
1135 cancer cells. *J. Androl.* **27**, 671–678.

1136 **Terman, G. W., Jin, W., Cheong, Y.-P., Lowe, J., Caron, M. G., Lefkowitz, R. J. and**
1137 **Chavkin, C.** (2004). G-protein receptor kinase 3 (GRK3) influences opioid analgesic
1138 tolerance but not opioid withdrawal. *Br. J. Pharmacol.* **141**, 55–64.

1139 **Thomas, P.** (2019). Membrane androgen receptors unrelated to nuclear steroid
1140 receptors. *Endocrinology* **160**, 772–781.

1141 **Thomas, P., Pang, Y., Dong, J. and Berg, A. H.** (2014). Identification and
1142 characterization of membrane androgen receptors in the ZIP9 zinc transporter
1143 subfamily: II. Role of human ZIP9 in testosterone-induced prostate and breast cancer
1144 cell apoptosis. *Endocrinology* **155**, 4250–4265.

1145 **Tilley, W. D., Marcelli, M., Wilson, J. D. and McPhaul, M. J.** (1989). Characterization
1146 and expression of a cDNA encoding the human androgen receptor. *Proc Natl Acad*
1147 *Sci U S A* **86**, 327–31.

1148 **Trapman, J., Klaassen, P., Kuiper, G. G., van der Korput, J. A., Faber, P. W., van**
1149 **Rooij, H. C., Geurts van Kessel, A., Voorhorst, M. M., Mulder, E. and Brinkmann,**
1150 **A. O.** (1988). Cloning, structure and expression of a cDNA encoding the human
1151 androgen receptor. *Biochem. Biophys. Res. Commun.* **153**, 241–248.

1152 **Travison, T. G., Vesper, H. W., Orwoll, E., Wu, F., Kaufman, J. M., Wang, Y.,**
1153 **Lapauw, B., Fiers, T., Matsumoto, A. M. and Bhasin, S.** (2017). Harmonized
1154 reference ranges for circulating testosterone levels in men of four cohort studies in
1155 the united states and europe. *J. Clin. Endocrinol. Metab.* **102**, 1161–1173.

1156 **Treviño, L. S. and Gorelick, D. A.** (2021). The interface of nuclear and membrane
1157 steroid signaling. *Endocrinology* **162**,.

1158 **Vyas, A. K., Hoang, V., Padmanabhan, V., Gilbreath, E. and Mietelka, K. A.** (2016).
1159 Prenatal programming: adverse cardiac programming by gestational testosterone
1160 excess. *Sci. Rep.* **6**, 28335.

1161 **Wang, Y., Tsui, H., Ke, Y., Shi, Y., Li, Y., Davies, L., Cartwright, E. J., Venetucci, L.,**
1162 **Zhang, H., Terrar, D. A., et al.** (2014). Pak1 is required to maintain ventricular Ca^{2+}
1163 homeostasis and electrophysiological stability through SERCA2a regulation in mice.
1164 *Circ. Arrhythm. Electrophysiol.* **7**, 938–948.

1165 **Westerfield, M.** (2000). *The Zebrafish Book. A Guide for the Laboratory Use of*
1166 *Zebrafish (Danio Rerio).* 4th ed. Eugene, OR: University of Oregon Press.

1167 **Whiting, K. P., Brain, P. F. and Restall, C. J.** (1995). Steroid hormone induced effects
1168 on membrane fluidity. *Biochem. Soc. Trans.* **23**, 438S.

1169 **Whiting, K. P., Restall, C. J. and Brain, P. F.** (2000). Steroid hormone-induced effects
1170 on membrane fluidity and their potential roles in non-genomic mechanisms. *Life Sci.*
1171 **67**, 743–757.

1172 **Wunderlich, F., Benten, W. P. M., Lieberherr, M., Guo, Z., Stamm, O., Wrehlke, C.,**
1173 **Sekeris, C. E. and Mossmann, H.** (2002). Testosterone signaling in T cells and
1174 macrophages. *Steroids* **67**, 535–538.

1175 **Wu, F. C. W., Tajar, A., Beynon, J. M., Pye, S. R., Silman, A. J., Finn, J. D., O'Neill,**
1176 **T. W., Bartfai, G., Casanueva, F. F., Forti, G., et al.** (2010). Identification of late-
1177 onset hypogonadism in middle-aged and elderly men. *N. Engl. J. Med.* **363**, 123–135.

1178 **Wu, R. S., Lam, I. I., Clay, H., Duong, D. N., Deo, R. C. and Coughlin, S. R.** (2018). A
1179 rapid method for directed gene knockout for screening in G0 zebrafish. *Dev. Cell* **46**,
1180 112-125.e4. Sciwheel inserting bibliography...

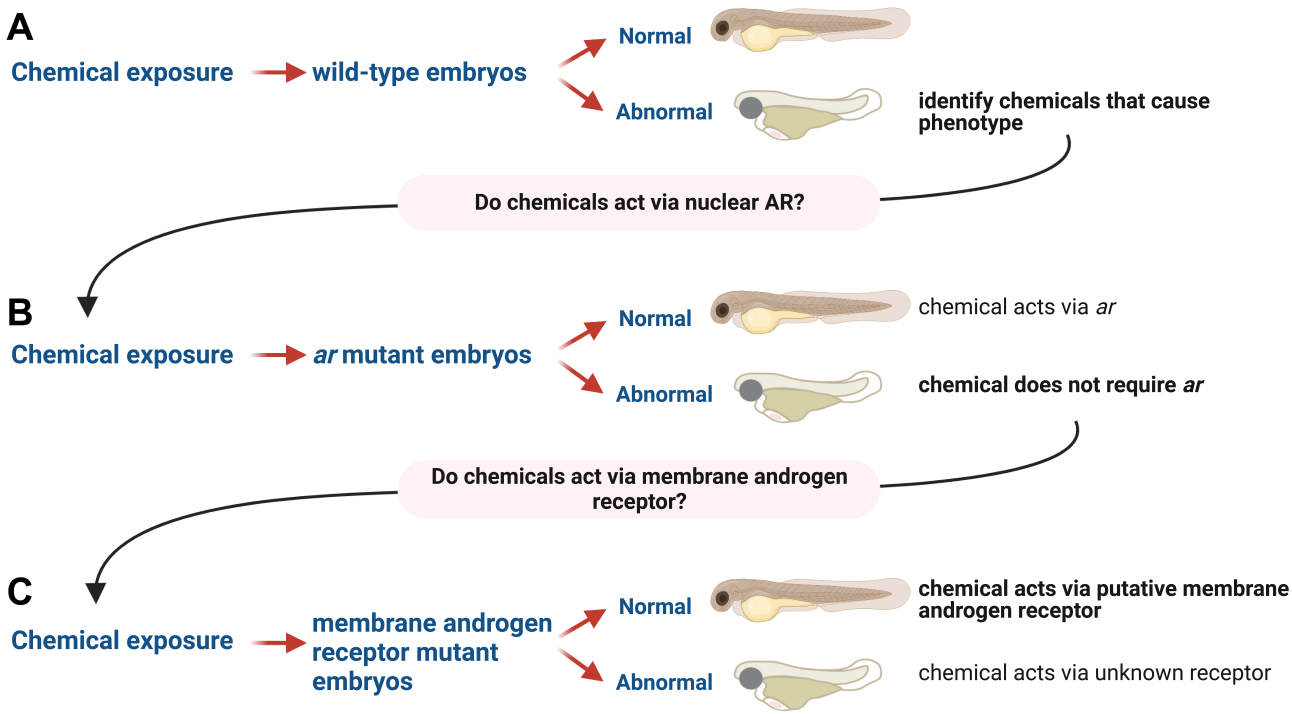

Figure 1. Chemical-genetic screen to identify receptors that mediate androgen-dependent phenotypes. **(A)** We exposed wild-type embryos to multiple androgens at different concentrations beginning at 3 hours post fertilization. We assayed embryo morphology at 2- and 3- days post fertilization. We identified chemicals that caused morphologic abnormalities. **(B)** We tested whether the phenotype is rescued in zebrafish with mutations in the nuclear androgen receptor gene (*ar*). If the phenotype is rescued, then the steroid acts via AR. **(C)** If the phenotype persists in the nuclear *ar* mutant, then we test zebrafish with mutations in membrane steroid receptors. To efficiently generate membrane androgen receptor mutants, we inject embryos with Cas9 and guide RNAs, expose injected embryos to chemicals, and screen for phenotypes. Following phenotypic screening, embryos are genotyped to determine mutation burden. Figure created using BioRender.com.

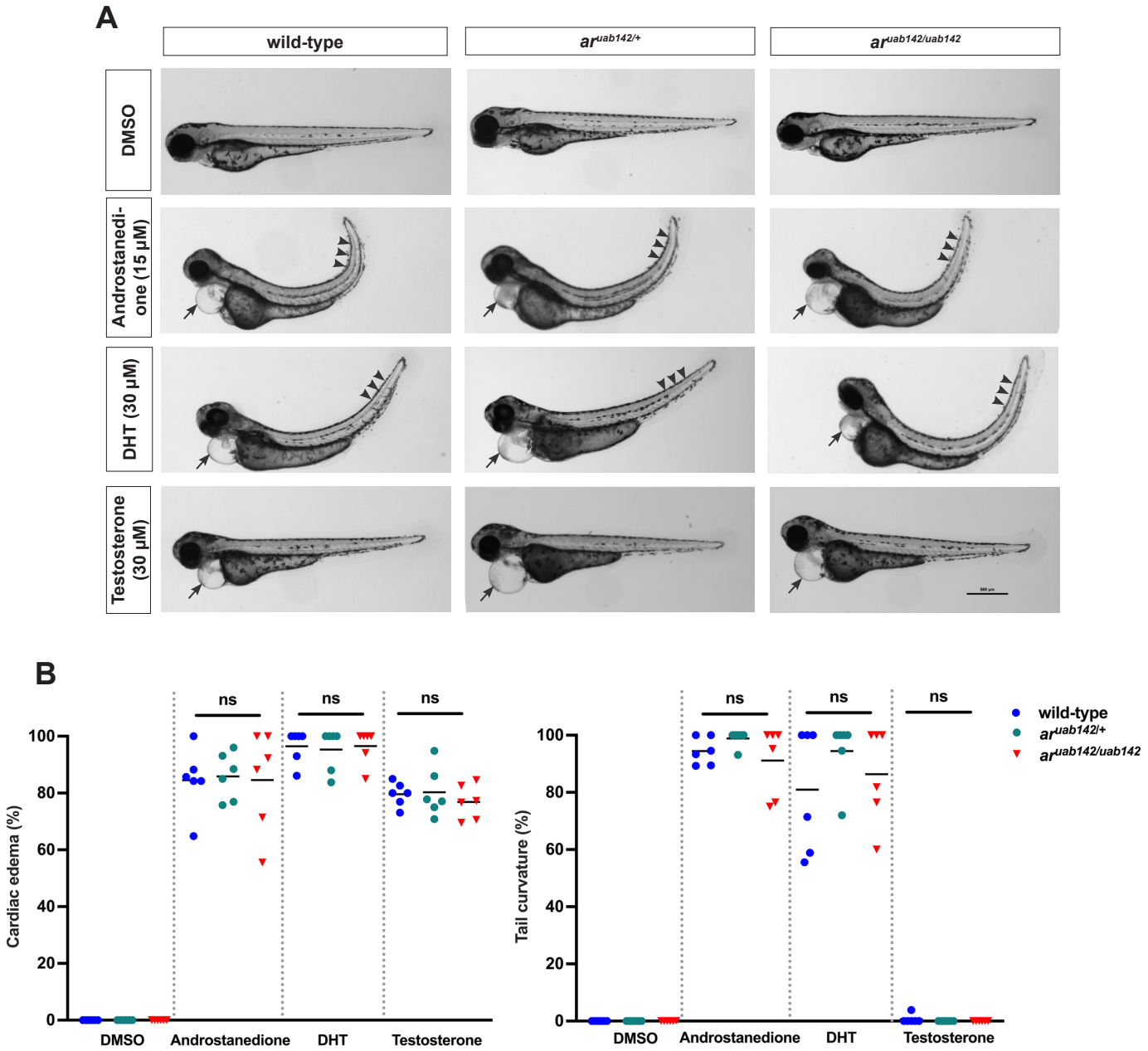

Figure 2. Identification of androgens that cause phenotypes in wild-type and nuclear androgen receptor (*ar*) mutant embryos. Wild-type or ar mutant embryos were exposed to vehicle (0.1% DMSO), 5α-Androstane-3,17-dione (androstanedione), dihydrotestosterone (DHT), or testosterone beginning at 3 hours post fertilization. (A) Representative images of embryos at 3 days post fertilization. Note cardiac edema (arrows) and tail curvature (arrowheads). Each clutch was derived from heterozygous parents and contained a mix of wild-type, heterozygous ar uab142/+, or homozygous ar uab142/uab142 embryos. Lateral views with anterior to the left, dorsal to the top. Scale bar = 500 µm. (B) Percent of embryos exhibiting cardiac edema or tail curvature. Each data point is the mean percent of embryos in a single clutch exhibiting cardiac edema or tail curvature (11-57 embryos per clutch). Clutches in the same treatment group were assayed on different days. Genotypes and treatments are separated by vertical gray dotted lines in each graph. Horizontal lines are the mean of each treatment. ns, not significant ($p > .05$), one-way ANOVA with Tukey's multiple comparisons test.

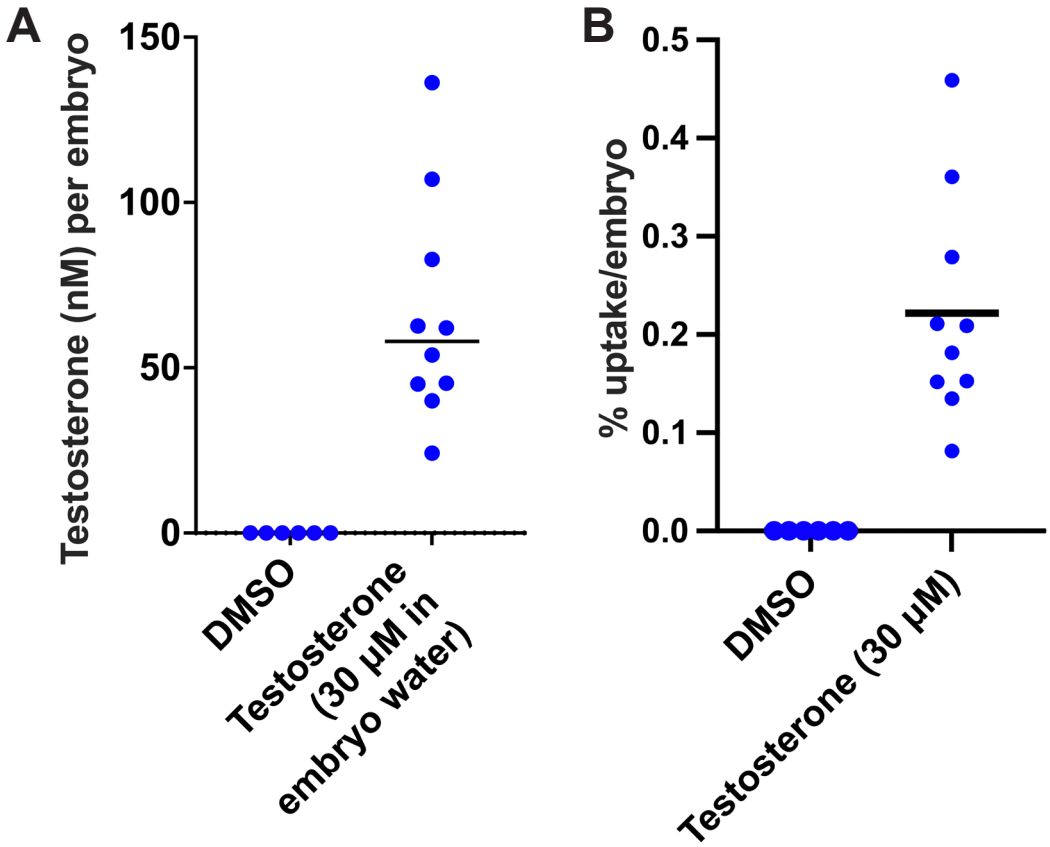

Figure 3. Testosteone concentration and uptake in zebrafish embryos. Wild-type embryos at 3 hours post fertilization (hpf) were exposed to vehicle (0.1% DMSO) or testosterone (30 µM) until 3 days post fertilization (dpf). Testosterone levels were measured using ELISA to calculate nM testosterone per embryo (A) and percent testosterone uptake per embryo (B). Each circle represents the mean testosterone concentrations or uptake per embryo for a single clutch of embryos, with 50 embryos pooled per clutch). Horizontal lines are the mean of each clutch.

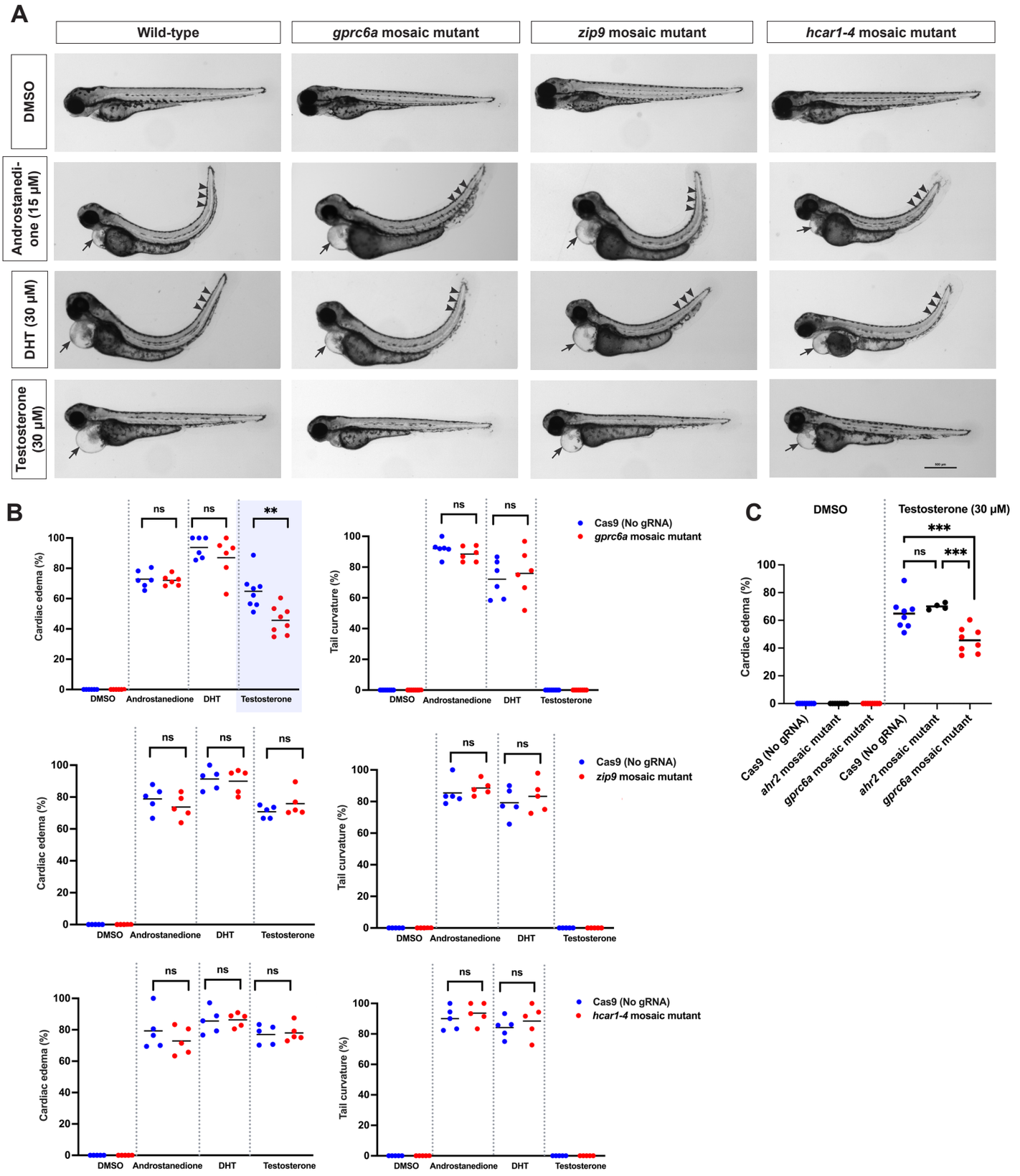

Figure 4. Testosterone phenotype is partially rescued by CRISPR targeting *gprc6a*. 1-cell stage embryos were injected with Cas9 protein alone or together with a cocktail of 4 guide RNAs targeting different regions of the indicated genes (*gprc6a*, *zip9*, *hcar1-4*). At 3 hours post fertilization, embryos were exposed to vehicle (0.1% DMSO), 5α-Androstane-3,17-dione (androstanedione), dihydrotestosterone (DHT), or testosterone. **(A)** Representative images of embryos at 3 days post fertilization. Note cardiac edema (arrows) and curved tail (arrowheads), except in *gprc6a* mosaic mutants following testosterone exposure. Lateral views with anterior to the left, dorsal to the top. Scale bars = 500 µm. **(B)** Percent of embryos exhibiting cardiac edema (left graphs) or tail curvature (right graphs). Each data point is the percent of embryos in a single clutch exhibiting cardiac edema or tail curvature (25-160 embryos per clutch). Clutches in the same treatment group were assayed on different days. Genotypes and treatments are separated by vertical gray dotted lines in each graph. Horizontal lines are the mean of each treatment. **(C)** As an additional control, embryos were injected with Cas9 protein alone or with guide RNAs targeting an unrelated gene *(ahr2),* and then exposed to vehicle or testosterone. The percent of embryos with cardiac edema was assayed at 3 days post fertilization. Each data point represents a single clutch (35-70 embryos per clutch). ns, not significant ($p > .05$), $^{**}p < .01$, $^{***}p < .001$, one-way ANOVA with Tukey's multiple comparisons test.

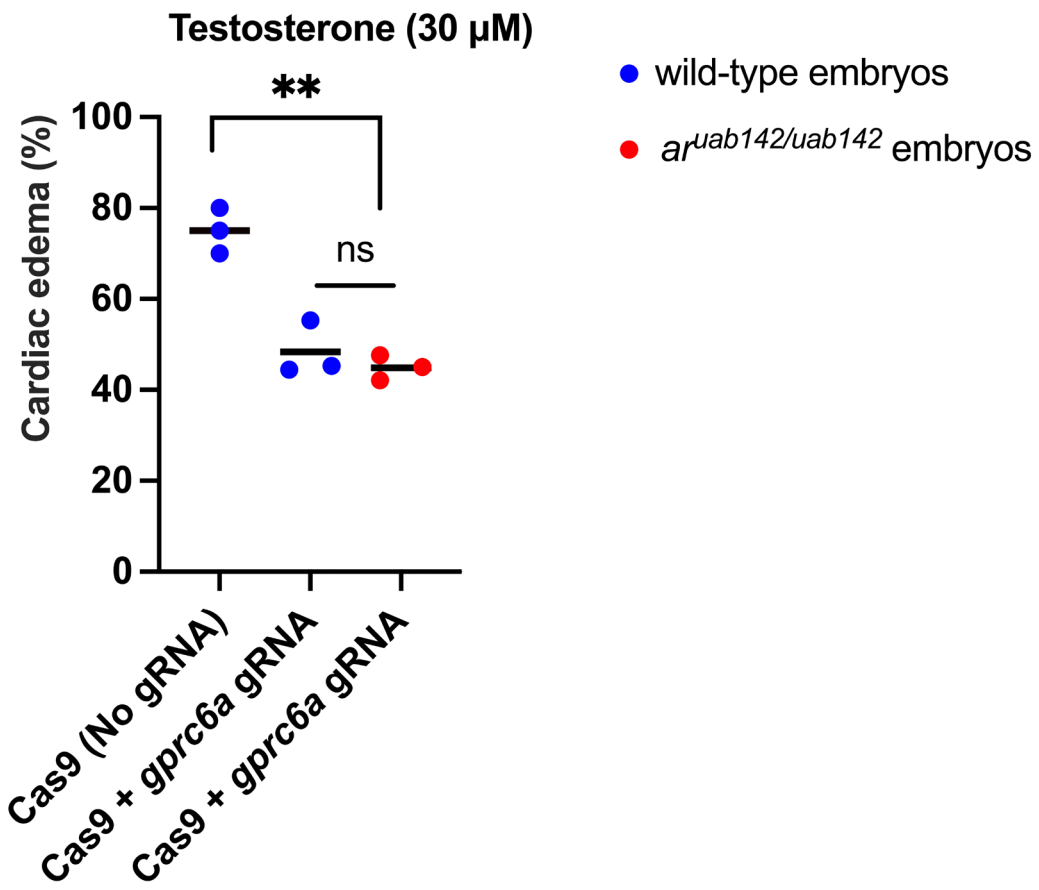

Figure 5. Testosterone phenotype in double mutants (*gprc6a* mosaic mutant + *ar*$^{uab142/uab142}$) is similar to *gprc6a* mosaic mutant. 1-cell stage ***ar***$^{uab142/uab142}$ embryos were injected with Cas9 protein alone or together with a cocktail of 4 guide RNAs targeting different regions of the *gprc6a* gene. At 3 hours post fertilization, embryos were exposed to testosterone. Morphologic phenotypes were assayed at 3 days post fertilization. Each data point is the mean percent of embryos in a single clutch exhibiting cardiac edema (19-80 embryos per clutch). Clutches in the same treatment group were assayed on different days. Horizontal lines are the mean of each group. **$p < .01$, ns, not significant ($p > .05$), one-way ANOVA with Tukey's multiple comparisons test.

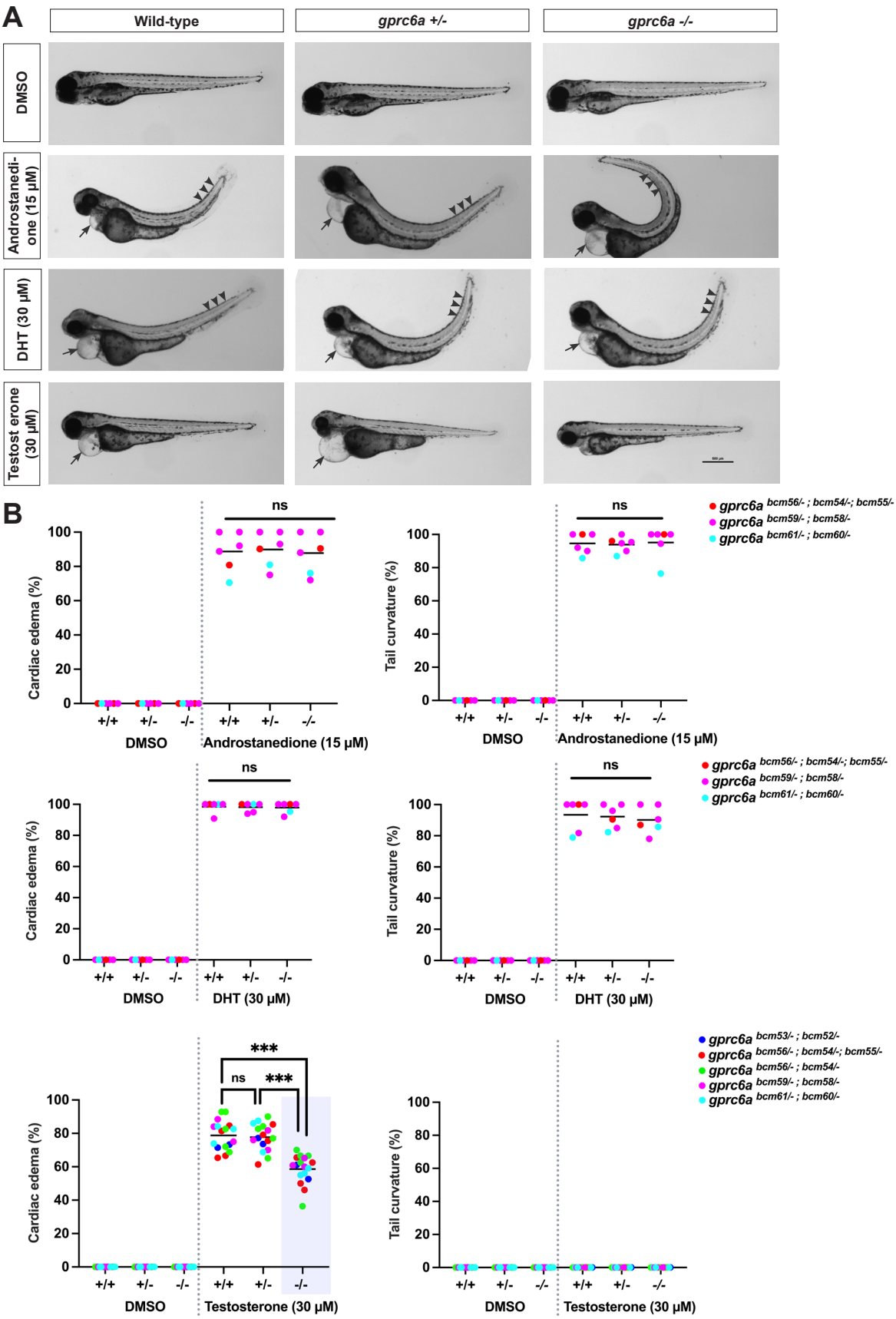

Figure 6. Testosterone phenotype is partially rescued in homozygous *gprc6a* mutants. Heterozygous *gprc6a* adult zebrafish were crossed to each other to generate zygotic *gprc6a* mutants. The clutch contained a mix of wild-type and mutant embryos (denoted as wild-type +/+, heterozygous +/-, or homozygous -/-). Embryos were exposed to vehicle (0.1% DMSO) or 5α-Androstane-3,17-dione (androstanedione), dihydrotestosterone (DHT), and testosterone beginning at 3 hours post fertilization. Morphologic phenotypes were assayed at 3 days post fertilization, then each embryo was genotyped. **(A)** Representative images of *gprc6a* $^{bcm56/-; bcm54/-; bcm55/-}$ embryos at 3 days post fertilization. Note cardiac edema (arrows) and curved tail (arrowheads), except in homozygous *gprc6a* mutants following testosterone exposure. Lateral views with anterior to the left, dorsal to the top. Scale bars = 500 µm. **(B)** Percent of embryos exhibiting cardiac edema (left graph) or tail curvature (right graph). Each data point is the mean percent of embryos in a single clutch exhibiting cardiac edema or tail curvature (15-50 embryos per clutch). Clutches in the same treatment group were assayed on different days. Horizontal lines are the mean of each group. Five independently generated zygotic mutant lines are shown, where each line is a different color and each allele designation indicates a unique DNA mutation. ***p < .001, ns, not significant (p > .05), one-way ANOVA with Tukey's multiple comparisons test.

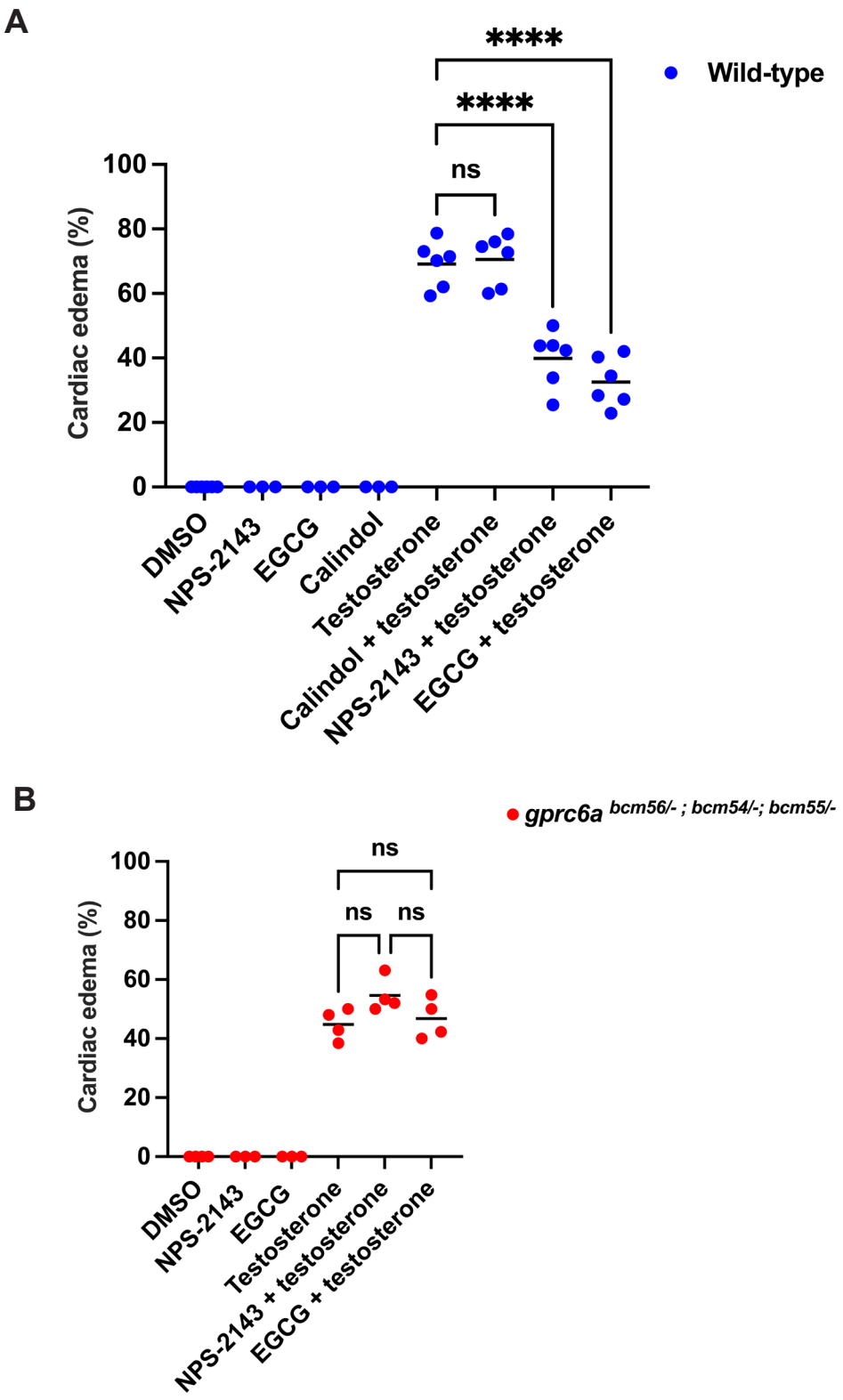

Figure 7. GPRC6A antagonists rescue testosterone phenotype in wild-type embryos but have no effect in *gprc6a* mutants. (A) Wild-type embryos were exposed to vehicle (0.1% DMSO) or GPRC6A antagonists: calindol (5 μM), NPS-2143 (5 μM), and epigallocatechin gallate (EGCG, 100 μM) with or without testosterone (30 μM) beginning at 3 hours post fertilization. Morphologic phenotypes were assayed at 3 days post fertilization. NPS-2143 and EGCG reduced cardiac edema following testosterone exposure. **(B)** Homozygous zygotic *gprc6a* mutant embryos were exposed to vehicle, NPS-2143 (5 μM), or EGCG (100 μM) with or without testosterone (30 μM) beginning at 3 hours post fertilization. Morphologic phenotypes were assayed at 3 days post fertilization. Antagonists failed to reduce cardiac edema in *gprc6a* mutant embryos. Each data point is the mean percent of embryos in a single clutch exhibiting cardiac edema (15-25 embryos per clutch). Clutches in the same treatment group were assayed on different days. Horizontal lines are the mean of each group. ****$p < .0001$, ns, not significant ($p > .05$), one-way ANOVA with Tukey's multiple comparisons test.

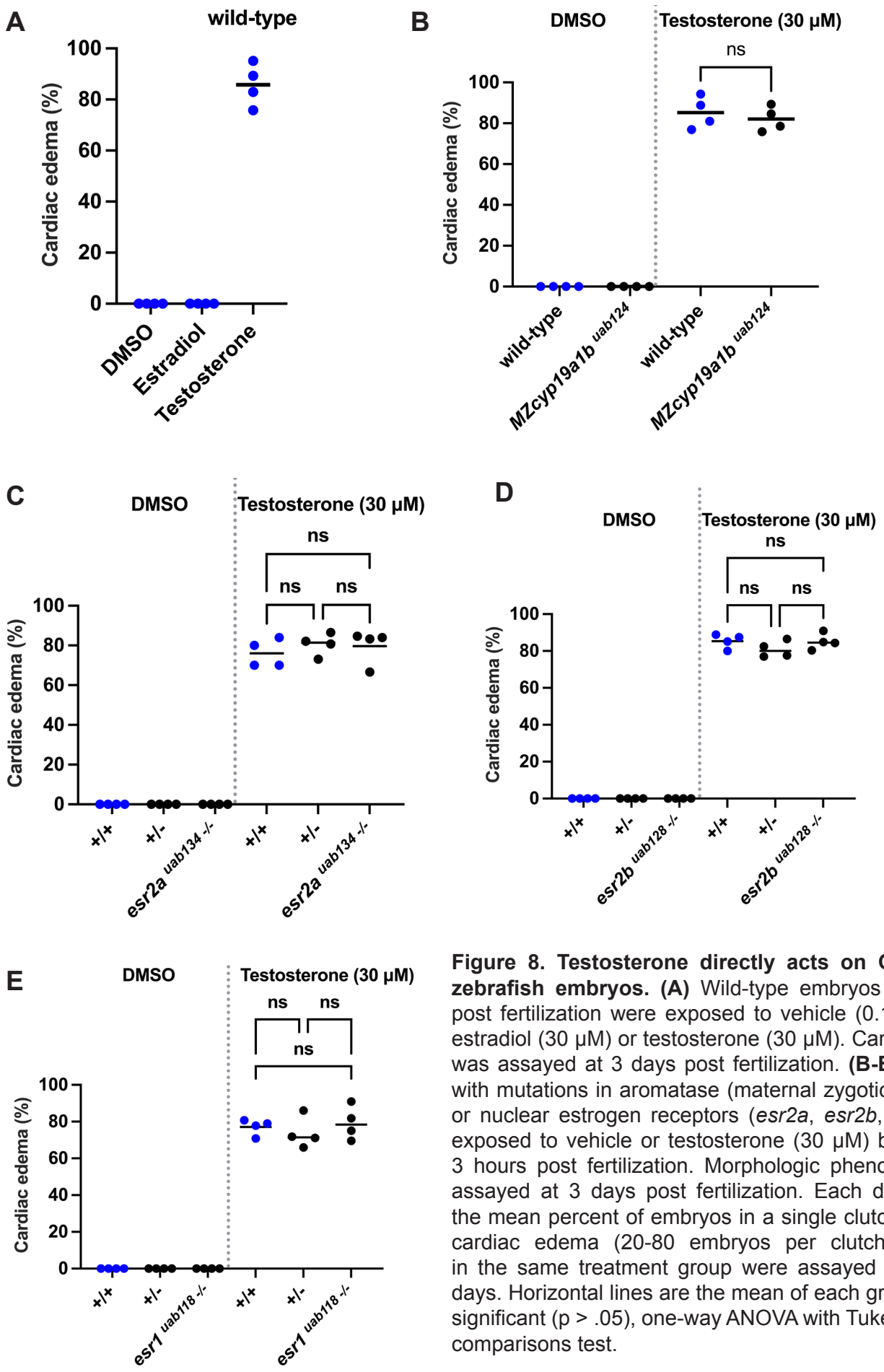

Figure 8. Testosterone directly acts on GPRC6A in zebrafish embryos. (A) Wild-type embryos at 3 hours post fertilization were exposed to vehicle (0.1% DMSO), estradiol (30 μM) or testosterone (30 μM). Cardiac edema was assayed at 3 days post fertilization. **(B-E)** Zebrafish with mutations in aromatase (maternal zygotic *cyp19a1b*) or nuclear estrogen receptors (*esr2a*, *esr2b*, *esr1*) were exposed to vehicle or testosterone (30 μM) beginning at 3 hours post fertilization. Morphologic phenotypes were assayed at 3 days post fertilization. Each data point is the mean percent of embryos in a single clutch exhibiting cardiac edema (20-80 embryos per clutch). Clutches in the same treatment group were assayed on different days. Horizontal lines are the mean of each group. ns, not significant ($p > .05$), one-way ANOVA with Tukey's multiple comparisons test.

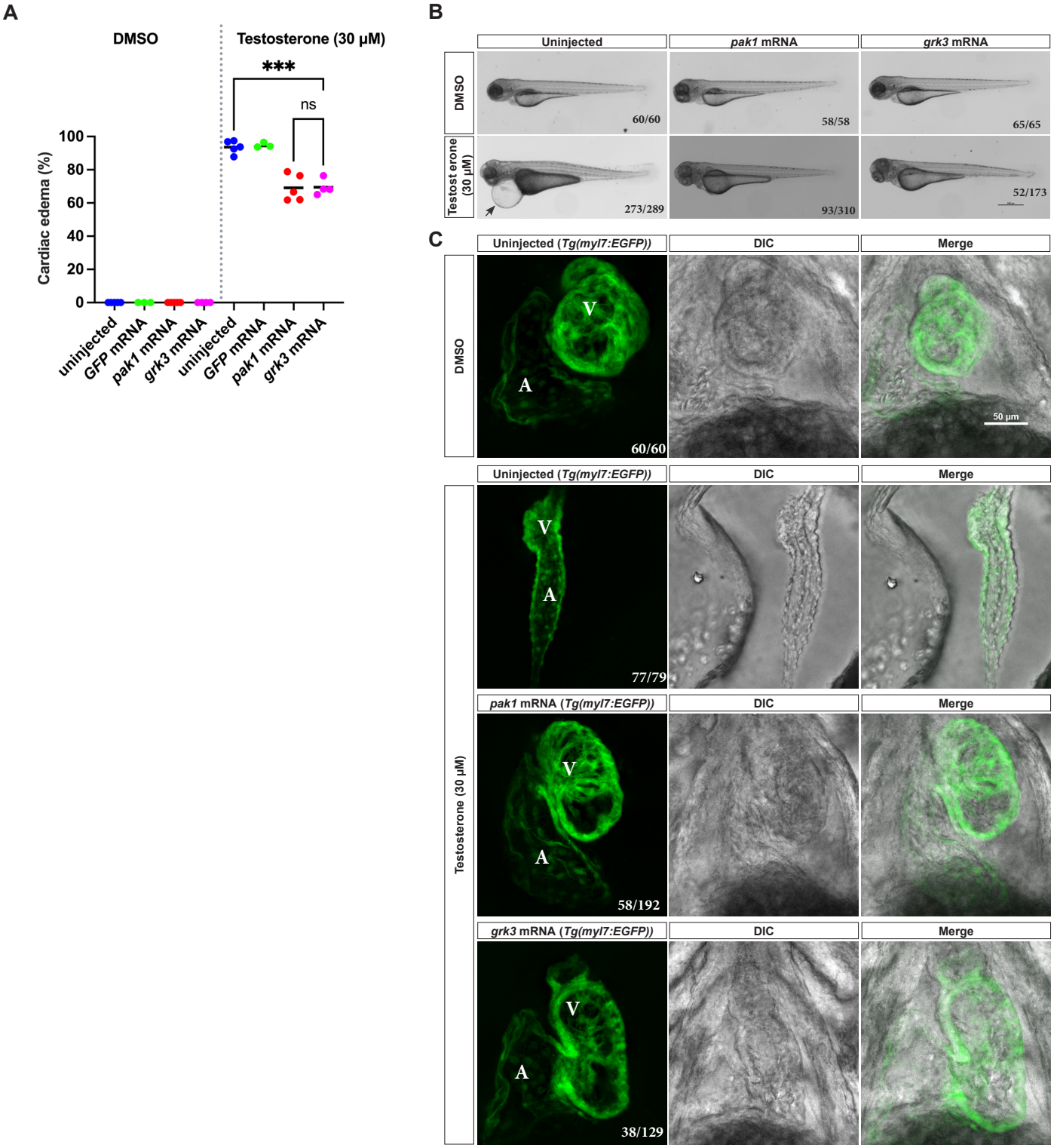

Figure 9. Testosterone phenotype is partially rescued by overexpression of *pak1* or *grk3* mRNA. (A) Wild-type embryos were injected with *gfp* mRNA, *pak1* mRNA, or *grk3* mRNA. Embryos were exposed to vehicle (0.1% DMSO) or testosterone (30 μM) beginning at 3 hours post fertilization (hpf). Morphologic phenotypes were assayed at 3 days post fertilization (dpf). *pak1* mRNA and *grk3* mRNA reduced cardiac edema following testosterone exposure, whereas *gfp* mRNA had no effect. Each data point is the mean percent of embryos in a single clutch exhibiting cardiac edema (29-71 embryos per clutch, 3-5 clutches per group). Clutches in the same treatment group were assayed on different days. Horizontal lines are the mean of each group. ****p < .0001, ns, not significant (p > .05), one-way ANOVA with Tukey's multiple comparisons test. **(B)** Representative brightfield images of embryos from (A) at 3 days post fertilization. Note cardiac edema (arrows). Lateral views with anterior to the left, dorsal to the top. Fractions in the bottom right corners refer to the number of embryos with the indicated phenotype over the total number of embryos examined. Scale bar = 500 μm. **(C)** Cardiac phenotypes examined on the background of *Tg(myl7:EGFP)* embryos after exposure to testosterone (30 μM) or vehicle controls (0.1% DMSO) beginning at 3 hpf. Representative confocal maximum intensity projections of live embryo hearts at 3 dpf. Fractions in the bottom right corners refer to the number of embryos with the indicated phenotype over the total number of embryos examined (30-75 embryos per clutch, 2-3 clutches per group). Myocardial cells are labeled in green, A = atrium, V = ventricle, DIC = differential interference contrast, Scale bar = 50 μm.

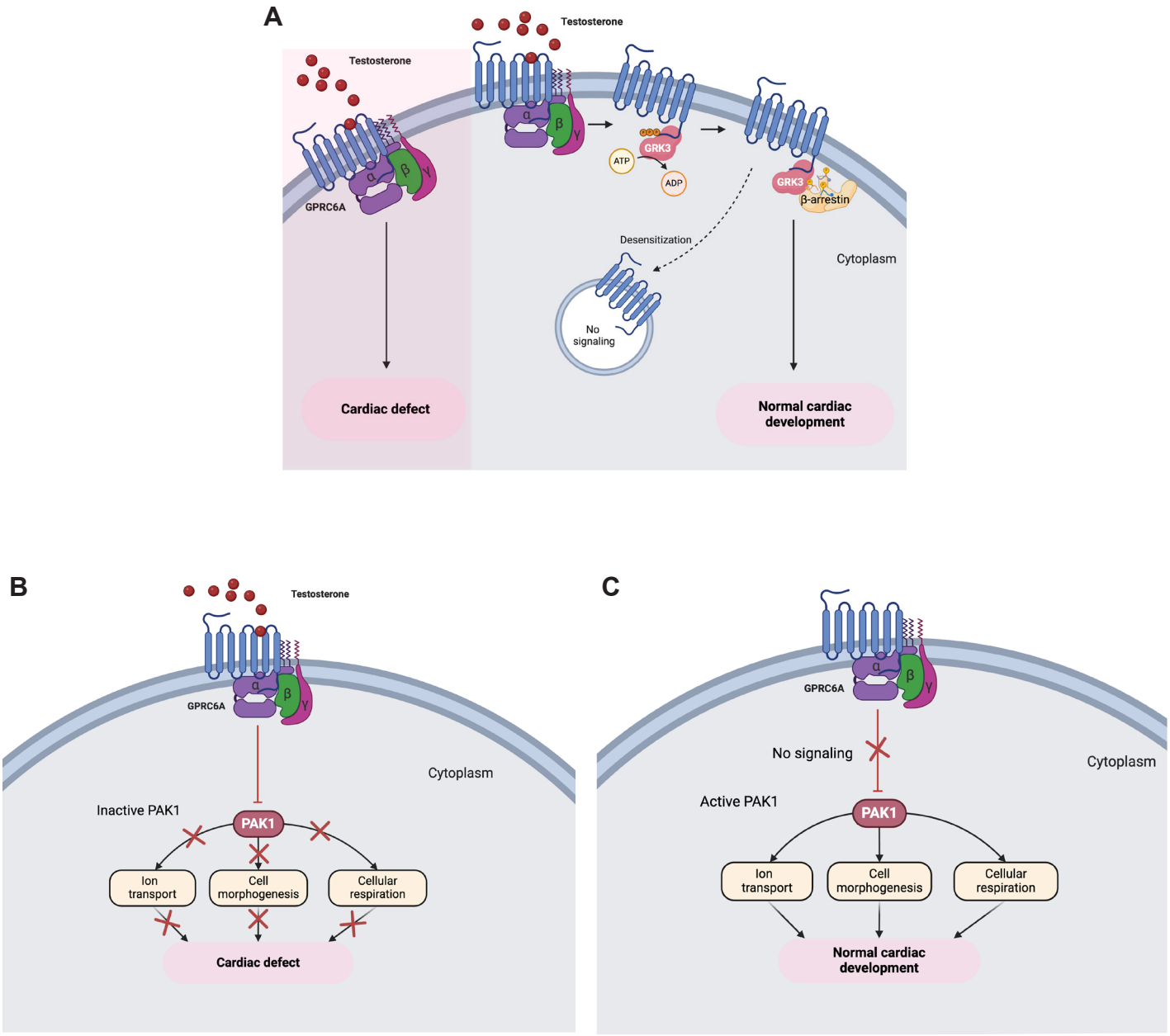

Figure 10. Model for GPRC6A-mediated signaling causing cardiac phenotype. **(A)** Testosterone activation of GPRC6A leads to activation of second messenger pathways that cause cardiac defects. The GPCR kinase GRK3 can reduce GPRC6A activity by promoting recruitment of β-arrestins, preventing G proteins from associating with GPRC6A, and increasing receptor internalization, blocking the effects of testosterone and restoring normal cardiac development. **(B)** Testosterone activation of GPRC6A inhibits or downregulates PAK1, thereby inactivating downstream signaling required for normal cardiac development. **(C)** In the absence of testosterone, GPRC6A is less active, so PAK1 is permitted to activate downstream signaling required for normal cardiac development.

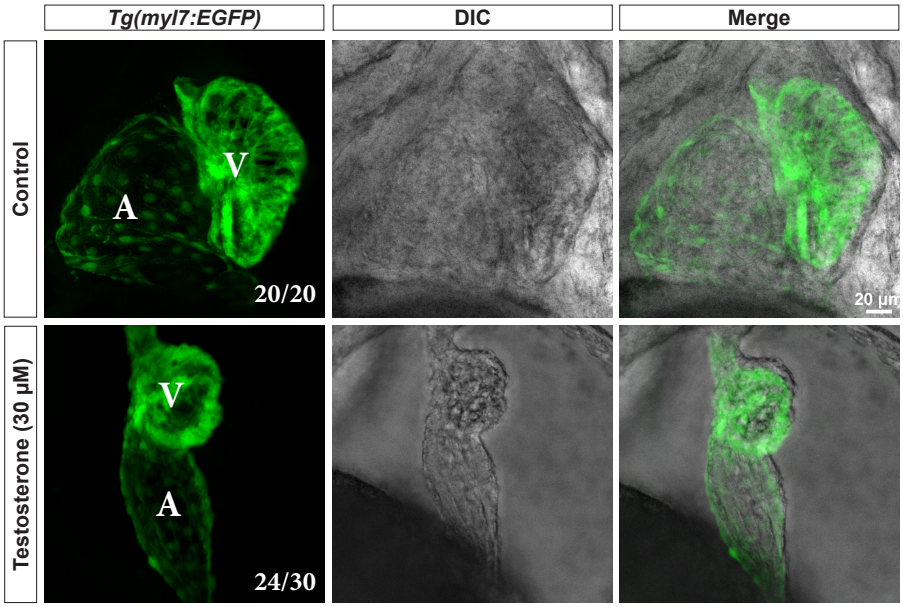

Figure S1. Testosterone exposure causes elongated atrium, shrunken ventricle and failure of heart looping. Confocal maximum intensity projections of live *Tg(myl7:EGFP)* embryos focused on the heart at 3 days post fertilization. Embryos were exposed to testosterone (30 µM) or vehicle control (0.1% DMSO) beginning at 3 hours post fertilization. 100% of control embryos had normal hearts (n=20), 80% of embryos exposed to testosterone had abnormal hearts (24 out of 30). Myocardial cells are labeled in green, A = atrium, V = ventricle, DIC = differential interference contrast.

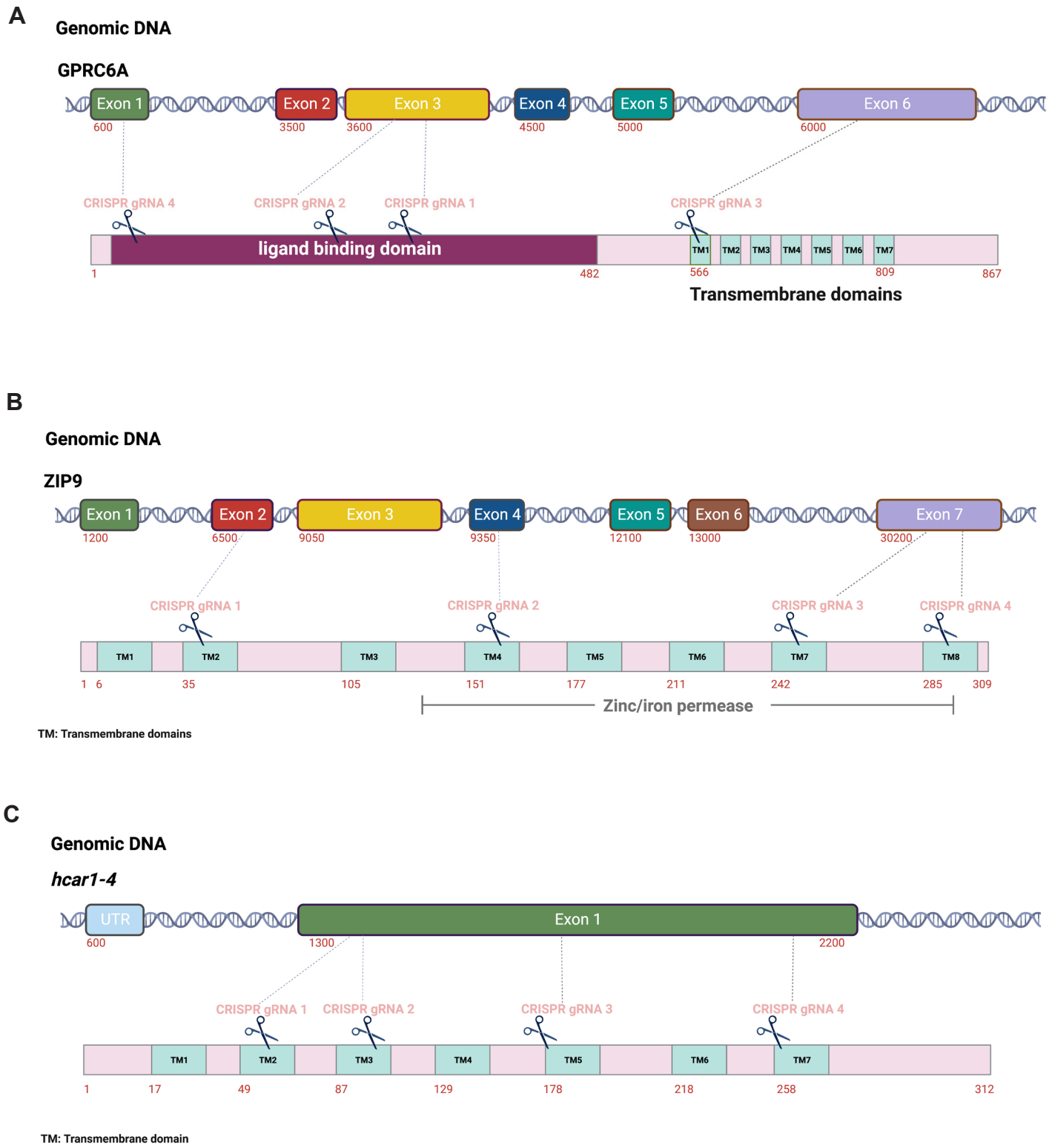

Figure S2. Location of guide RNAs targeting putative membrane androgen receptor genes. Four guide RNAs each were used to target *gprc6a* (**A**), *zip9* (**B**), and *hcar1-4* (**C**) genes. The predicted location in the corresponding protein is shown below each genomic DNA. Numbers indicate the starting and ending nucleotides of exons in the genomic DNA or amino acid numbers in the protein sequence. Boxes in the protein sequence indicate key structural or functional domains. Figure created using Biorender.com.

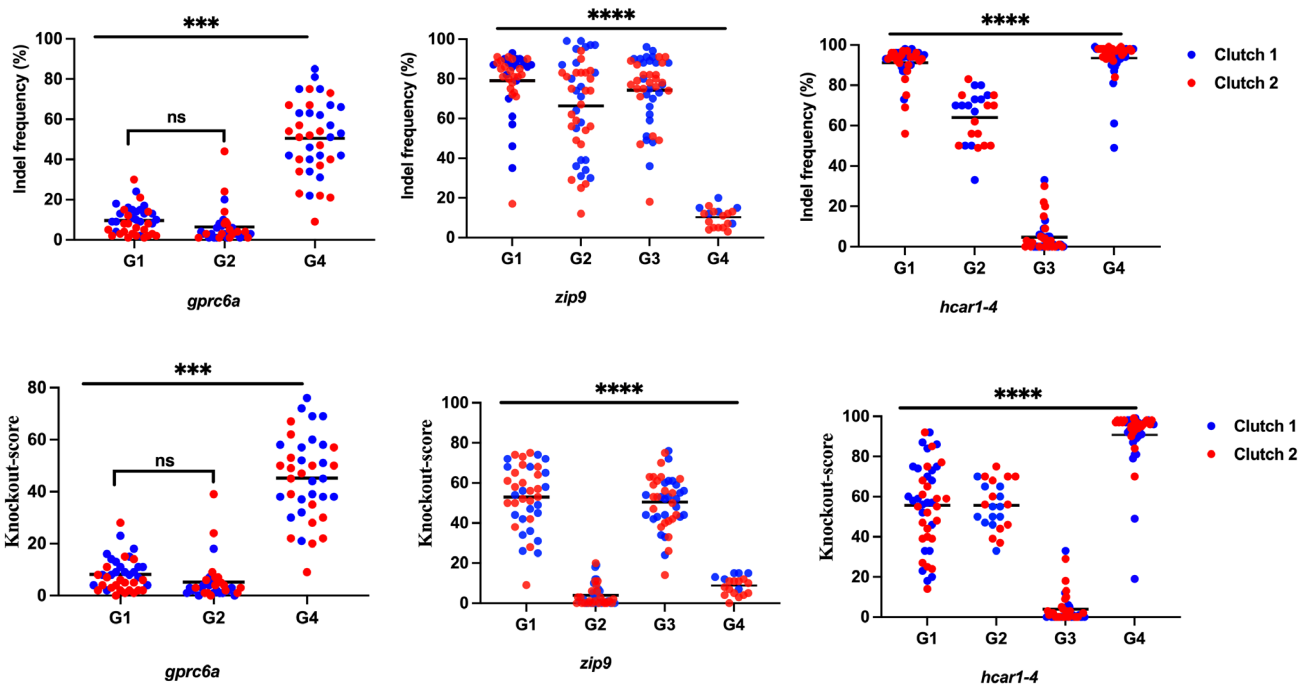

Figure S3. Multiplexed gRNA injection results in frequent mutations in injected embryos. 1-cell stage zebrafish embryos were injected with Cas9 protein together with a cocktail of 4 guide RNAs (gRNA 1 = G1; gRNA 2 = G2; gRNA 3 = G3; gRNA 4 = G4) targeting different regions of the indicated genes (*gprc6a, zip9, hcar-1-4*). At 1 day post fertilization, we harvested genomic DNA from each embryo individually, performed PCR to amplify each of the 4 different regions targeted by each guide RNA, and then we Sanger sequenced each PCR product. Sanger sequence was deconvoluted and analyzed using the ICE (Inference of CRISPR Edits) algorithm. Top graphs, percent of sequence from each embryo that has a mutation (indel frequency). Bottom graphs, percent of mutations in sequencing reactions from each embryo predicted to produce a non-functional protein (knockout score). Each data point represents sequencing results from a single embryo. Data points of the same color represent embryos from the same clutch, embryos that were produced from the same parents and injected and assayed together on the same day. Horizontal lines are the mean for each group. G3 targeting *gprc6a* produced no mutations and is not shown. ***$p < .001$, ****$p < .0001$, ns, not significant ($p > .05$), one-way ANOVA with Tukey's multiple comparisons test.

A **Genomic DNA**

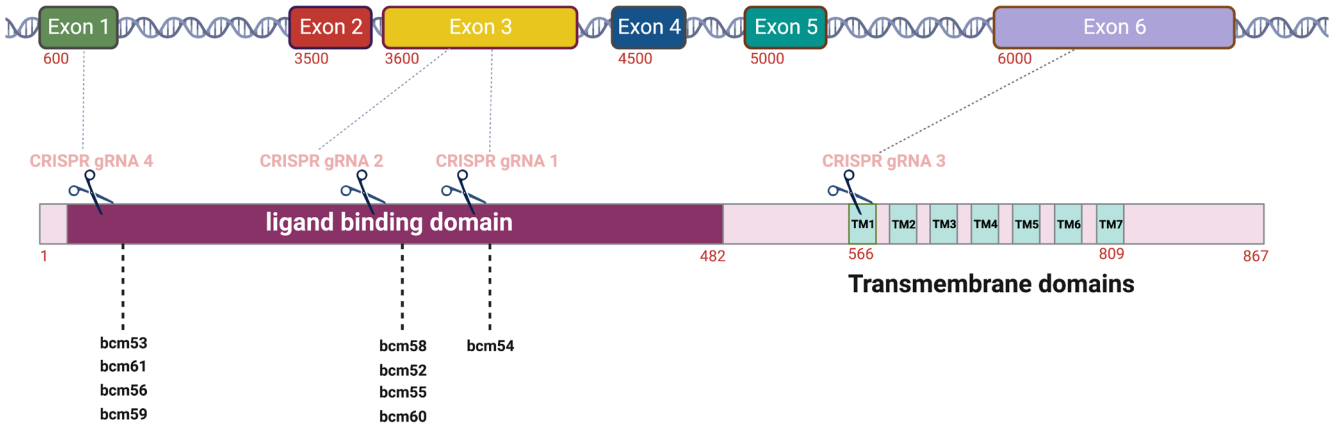

B

```
wild-type: ACTTTTCCCCATCCATGAGGCAGTGGTGCCAGTAAACTACACCGGCAACAACAGCATCTC
bcm53:     ACTTTTCCCCATCC-TGAGGCAGTGGTGCCAGTAAACTACACCGGCAACAACAGCATCTC -1 bp
bcm61:     ACTTTTCCCCATCCA----GCAGTGGTGCCAGTAAACTACACCGGCAACAACAGCATCTC -4 bp
bcm56:     ACTTTTCCCCA-----------GTGGTGCCAGTAAACTACACCGGCAACAACAGCATCTC -11 bp
bcm59:     ACTTTTCCCCATCCATGAGGCAG-----CCAGTAAACTACACCGGCAACAACAGCATCTC -5 bp

wild-type: ATTACAGATGGAGATTATGGACGTTCTGCCTTGGAAGGTTTCATACAGCACACCGAAACG
bcm52:     ATTACAGATGGAGATTATGGACGTTCTGCCTT-GAAGGTTTCATACAGCACACCGAAACG -1 bp
bcm55:     ATTACAGATGGAGATTATGGACGTTCTGCCT-GGAAGGTTTCATACAGCACACCGAAACG -1 bp
bcm60:     ATTACAGATGGAGATTATGGACGTTCTGCCTTGGAAGGT----------------AAACG -16 bp
bcm58:     ATTACAGATGGAGATTATGAGATTATGACGTTCTGCCTTGGAAGGTTTCATACAGCACACCGAAACG +7

wild-type: CACCTTGAACATCATTGAAAACAATCCGAAAGTTAGAGTGGTGATCTCGTTTGCTAAATC
bcm54:     CACCTTGAACATCATTGAAAACAAT-------TTAGAGTGGTGATCTCGTTTGCTAAATC -7 bp
```

C

```
Amino acid sequence (star indicates stop codon, red indicates missense amino acids)

                11                                                  60
wild-type:AGLMKVAEASIAQFSQLGASAPGNIIIGGLFPIHEAVVPVNYTGNNSISA 50 amino acids
bcm53:    AGLMKVAEASIAQFSQLGASAPGNIIIGGLFPILRQWCQ*TTPATTASLP frameshift at 44, premature stop at 50
bcm61:    AGLMKVAEASIAQFSQLGASAPGNIIIGGLFPIQQWCQ*TTPATTASLPL frameshift at 44, premature stop at 49
bcm56:    AGLMKVAEASIAQFSQLGASAPGNIIIGGLFPSGASKLHRQQQHLCP*AS frameshift at 43, premature stop at 58
bcm59:    AGLMKVAEASIAQFSQLGASAPGNIIIGGLFPIHEAVSKLHRQQQHLCP* frameshift at 48, premature stop at 60

                211                                                 260
wild-type:WVGIIITDGDYGRSALEGFIQHTETEGICIAFKAILPDSLADQQKLNTDI 50 amino acids
bcm52:    WVGIIITDGDYGRSLWKVSYSTPKRREFASPLKQSFQTH*QINRN*   frameshift at 225, premature stop at 250
bcm55:    WVGIIITDGDYGRSAWKVSYSTPKRREFASPLKQSFQTH*QINRN*TQ frameshift at 226, premature stop at 250
bcm60:    WVGIIITDGDYGRSALEGKRREFASPLKQSFQTH*QINRN*TQTSKTP frameshift at 229, premature stop at 245
bcm58:    WVGIIITDGDYGDYTFCLGRFHTAHRNGGNLHRL*SNPSRLTSRSTET frameshift at 223, premature stop at 245

                261                                                 310
wild-type:ENTLNIIENNPKVRVVISFAKSSQMQLLFKGLQSRNISNNMVWVASDNWS 50 amino acids
bcm54:    ENTLNIIENNLEW*SRLLNPLKCSCYLRGCRVETFQITWCGLPVITG  frameshift at 271, premature stop at 274
```

Figure S4. Generation of heritable *gprc6a* mutant zebrafish. **(A)** We generated heritable mutant alleles for *gprc6a* using CRISPR/Cas9. **(A)** 1-cell stage embryos were injected with 4 gRNAs targeting sites within exons 1, 3 and 6 of *gprc6a* (gray dotted lines). Injected embryos were raised to adulthood and crossed to wild-type zebrafish. Resulting progeny were raised to adulthood. We used PCR and Sanger sequencing to identify heterozygotes with putative loss-of-function mutations in the predicted protein, illustrated below the genomic DNA. Zebrafish containing desirable mutations were given allele designations (*bcm53*, *bcm61*, *bcm56*, *bcm59*, *bcm58*, *bcm52*, *bcm55*, *bcm60*, *bcm54*) and propagated. Numbers indicate the starting and ending nucleotides of exons in the genomic DNA or amino acid numbers in the protein sequence. Boxes in the protein sequence indicate key structural or functional domains. **(B)** Nucleotide sequence for each allele was confirmed by Sanger sequencing. Red dashes indicate deletions, green nucleotides indicate insertions. (**C)** Predicted changes to amino acid sequence for each allele. Red indicates amino acid mutations, asterisk indicates premature stop.

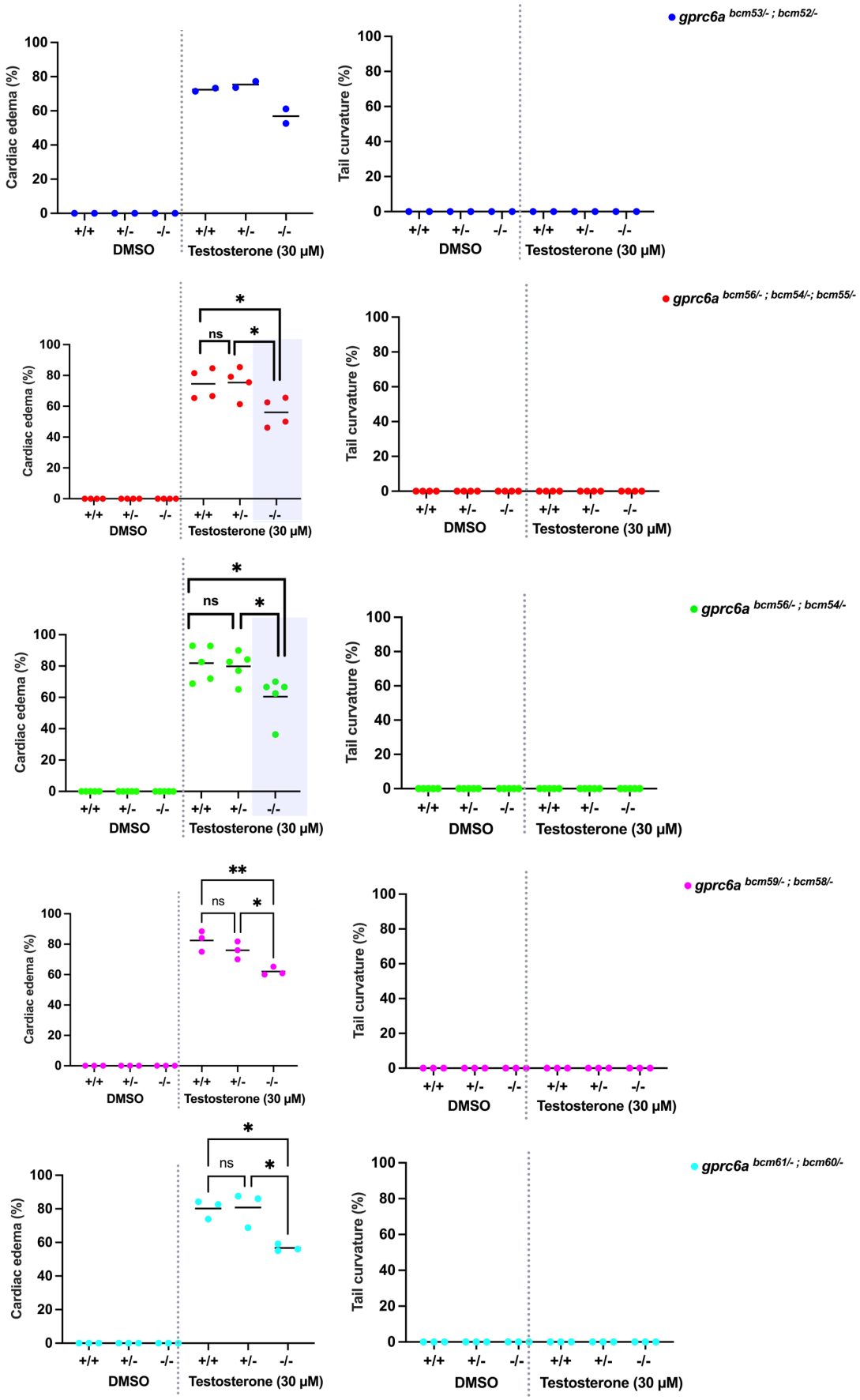

Figure S5. Testosterone phenotypes in homozygous *gprc6a* mutant embryos based on allele. Percent of embryos exhibiting cardiac edema (left graphs) or tail curvature (right graphs) phenotypes. Each data point is the mean percent of embryos in a single clutch exhibiting cardiac edema or tail curvature (15-50 embryos per clutch). Clutches in the same treatment group were assayed on different days. Horizontal lines are the mean of each group. This is the same data from Figure 6B but each allele is graphed separately. Genotypes and treatments are separated by vertical gray dotted lines in each graph. * $p < .05$, ** $p < .01$, ns, not significant ($p > .05$), one-way ANOVA with Tukey's multiple comparisons test.

A

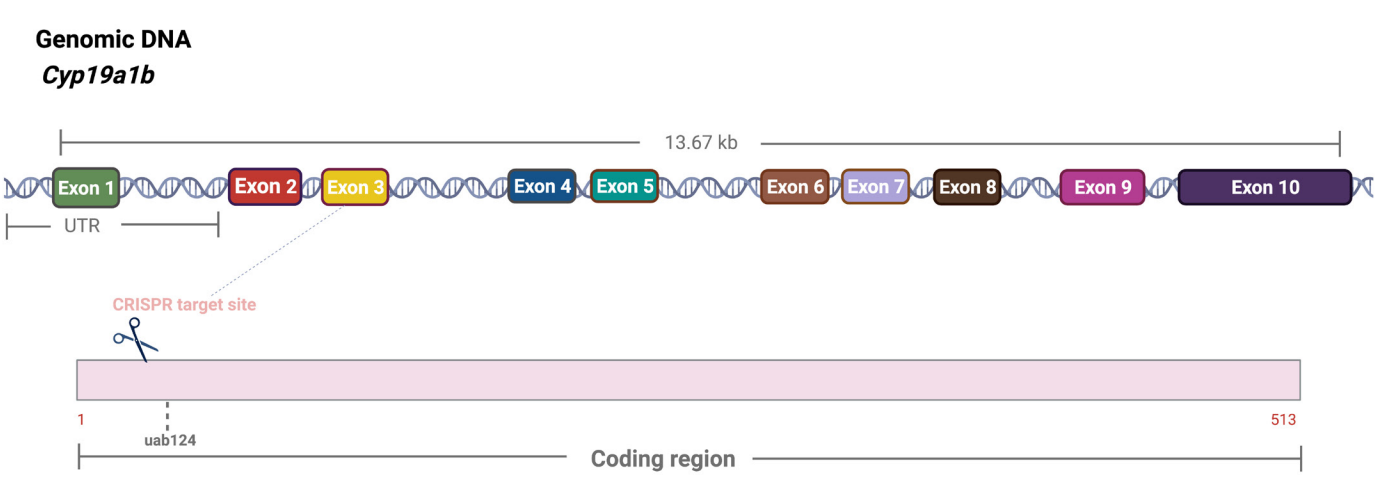

B

```
wild-type: TTCCCTGCACCACAGCGCCGATGTTTACCGCA--------------------TCCTTTACCACATGCTCCATCATCACC
uab124:    TTCCCTGCACCACAGCGCCGATGTTTACCGCAGCTTACAGACATCCTTAAACTCCTTTACCACATGCTCCATCATCACC +20

Amino acid sequence (star indicates stop codon, red indicates missense amino acids)
           1                                                  50
wild-type: MMEHVVKDAVNIGAVVQGTLLLLTGTLMLILLHRIFGVKNWRNQSALPGP 50 amino acids
uab124:    MMEHVVKDAVLTDILKQTSALWCREHYCC*                    frameshift at 11
                                                             premature stop at 30
```

Figure S6. Generation of *cyp19a1b* mutant zebrafish.
We generated heritable mutant alleles for *cyp19a1b* using CRISPR/Cas9. **(A)** 1-cell stage embryos were injected with gRNA targeting exon 3 of *cyp19a1b* (gray dotted lines). Injected embryos were raised to adulthood and crossed to wild-type zebrafish. Resulting progeny were raised to adulthood, where we identified allele *uab124*. Numbers indicate the starting and ending amino acid numbers in the protein sequence. **(B)** *uab124* nucleotide sequence was confirmed by Sanger sequencing. Green nucleotides indicate insertions. Predicted changes to amino acid sequence are also indicated. Red indicates amino acid mutations, and asterisk indicates premature stop.

Genotype	Clutch (biological replicate)	Treatment	Number of embryos/clutch	% Cardiac edema, 3 dpf	Mean % embryos with cardiac edema	Standard deviation (cardiac edema)	% Tail curvature, 3 dpf	Mean % embryos with tail curvature	Standard deviation (tail curvature)	% Cardiac edema + tail curvature, 3 dpf	% Normal embryos, 3 dpf	Notes
Wild-type	n = 6	0.1% DMSO	12,10,12,14,10,10	0,0,0,0,0,0	0	0	0,0,0,0,0,0	0	0	0,0,0,0,0,0	100,100,100,100,100,000	Pictured in Fig. 2
Heterozygous *ar* $^{uab142/+}$	n = 6	0.1% DMSO	25,24,22,26,23,25	0,0,0,0,0,0	0	0	0,0,0,0,0,0	0	0	0,0,0,0,0,0	100,100,100,100,100,000	Pictured in Fig. 2
homozygous *ar* $^{uab142/uab142}$	n = 6	0.1% DMSO	10,12,11,10,14,10	0,0,0,0,0,0	0	0	0,0,0,0,0,0	0	0	0,0,0,0,0,0	100,100,100,100,100,000	Pictured in Fig. 2
Wild-type	n = 6	15 µM androstanedione	15,19,15,19,17,12	64,84,85,84,88,100	84	12	94,89,89,100,100,93	94	5	64,84,85,84,88,100	6,11,11,0,0,0	Pictured in Fig. 2
Heterozygous *ar* $^{uab142/+}$	n = 6	15 µM androstanedione	33,26,29,39,25,20	75,88,93,76,96,85	86	9	100,100,93,100,100,100	99	3	75,88,93,76,96,85	0,0,7,0,0,0	Pictured in Fig. 2
homozygous *ar* $^{uab142/uab142}$	n = 6	15 µM androstanedione	17,12,13,21,17,13	88,100,55,71,100,92	84	16	76,75,100,95,100,100	91	11	88,100,55,71,100,92	12,0,0,5,0,0	Pictured in Fig. 2
Wild-type	n = 6	30 µM DHT	20,27,25,18,20,13	86,92,100,100,100,100	96	5	55,58,71,100,100,100	81	20	86,92,100,100,100,100	14,8,0,0,0,0	Pictured in Fig. 2
Heterozygous *ar* $^{uab142/+}$	n = 6	30 µM DHT	37,57,50,48,48,25	83,100,88,100,100,100	95	7	94,100,72,100,100,100	94	10	83,100,88,100,100,100	6,0,12,0,0,0	Pictured in Fig. 2
homozygous *ar* $^{uab142/uab142}$	n = 6	30 µM DHT	20,25,15,20,22,13	85,100,94,100,100,100	97	6	60,81,76,100,100,100	86	15	85,100,94,100,100,100	15,0,6,0,0,0	Pictured in Fig. 2
Wild-type	n = 6	30 µM Testosterone	15,23,26,20,26,20	80,82,76,85,73,80	79	4	0,0,0,0,0,0	0	0	0,0,0,0,0,0	20,17,23,15,26,20	Pictured in Fig. 2
Heterozygous *ar* $^{uab142/+}$	n = 6	30 µM Testosterone	50,36,39,48,40,48	86,77,94,70,75,77	80	8	0,0,0,0,0,0	0	0	0,0,0,0,0,0	14,22,5,29,25,22	Pictured in Fig. 2
homozygous *ar* $^{uab142/uab142}$	n = 6	30 µM Testosterone	13,17,23,23,30,22	84,70,69,82,76,77	76	6	0,0,0,0,0,0	0	0	0,0,0,0,0,0	15,29,30,17,23,22	Pictured in Fig. 2

Table 1. Embryo data accompanying Figure 2.

Genotype	Clutch (biological replicate)	Treatment	Number of embryos/clutch	% Cardiac edema, 3 dpf	Mean % embryos with cardiac edema	Standard deviation (cardiac edema)	% Tail curvature, 3 dpf	Mean % embryos with tail curvature	Standard deviation (tail curvature)	% Cardiac edema + tail curvature, 3 dpf	% Normal embryos, 3 dpf	Notes
wild-type	n = 6	0.1% DMSO	22,24,10,22,22,24	0,0,0,0,0,0	0	0	0,0,0,0,0,0	0	0	0,0,0,0,0,0	100,100,100,100,100,100,	Pictured in Fig. 3
gprc6a mosaic mutant	n = 6	0.1% DMSO	10,10,22,14,24,22	0,0,0,0,0,0	0	0	0,0,0,0,0,0	0	0	0,0,0,0,0,0	100,100,100,100,100,100,	Pictured in Fig. 3
ahr2 mosaic mutant	n = 4	0.1% DMSO	24,12,22,16	0,0,0,0	0	0	0,0,0,0	0	0	0,0,0,0	100,100,100,100,	Pictured in Fig. 3
Wild-type	n = 5	0.1% DMSO	14,20,10,22,20	0,0,0,0,0	0	0	0,0,0,0,0	0	0	0,0,0,0,0	100,100,100,100,100,	Pictured in Fig. 3
zip9 mosaic mutant	n = 5	0.1% DMSO	11,10,22,14,14	0,0,0,0,0	0	0	0,0,0,0,0	0	0	0,0,0,0,0	100,100,100,100,100,	Pictured in Fig. 3
Wild-type	n = 5	0.1% DMSO	12,10,10,22,20	0,0,0,0,0	0	0	0,0,0,0,0	0	0	0,0,0,0,0	100,100,100,100,100,	Pictured in Fig. 3
hcar1-4 mosaic mutant	n = 5	0.1% DMSO	23,22,20,20,14	0,0,0,0,0	0	0	0,0,0,0,0	0	0	0,0,0,0,0	100,100,100,100,100,	Pictured in Fig. 3
wild-type	n = 6	15 µM androstanedione	115,32,50,36,36,26	78,68,72,80,72,65	73	6	93,100,92,91,83,92	92	5	78,68,72,80,72,65	7,0,8,9,17,8	Pictured in Fig. 3
gprc6a mosaic mutant	n = 6	15 µM androstanedione	38,34,34,36,36,38	68,73,68,77,72,71	72	3	86,94,93,83,83,89	88	5	68,73,68,77,72,71	14,6,7,17,17,11	Pictured in Fig. 3
Wild-type	n = 5	15 µM androstanedione	36,30,33,30,33	80,66,87,83,75	78	8	100,83,78,83,81	85	9	80,66,87,83,75	0,17,13,17,19	Pictured in Fig. 3
zip9 mosaic mutant	n = 5	15 µM androstanedione	48,36,40,40,36	79,83,70,72,63	73	8	95,86,90,87,83	88	5	79,83,70,72,63	5,14,10,13,17	Pictured in Fig. 3
Wild-type	n = 5	15 µM androstanedione	36,30,30,34,36	80,100,70,76,69	79	13	83,90,100,82,94	90	8	80,100,70,76,69	17,0,0,18,6	Pictured in Fig. 3
hcar1-4 mosaic mutant	n = 5	15 µM androstanedione	3,30,35,36,35	63,83,65,80,71	72	9	100,93,100,83,91	93	7	63,83,65,80,71	0,7,0,7,9	Pictured in Fig. 3
wild-type	n = 6	30 µM DHT	93,46,48,36,30,36	90,86,85,100,100,100	94	7	59,67,58,83,86,77	72	12	90,86,85,100,100,100	10,14,15,0,0,0	Pictured in Fig. 3
gprc6a mosaic mutant	n = 6	30 µM DHT	27,40,36,40,36,31	62,90,80,95,100,93	87	14	51,87,66,75,77,96	75	16	62,90,80,95,100,93	38,10,20,5,0,4	Pictured in Fig. 3
Wild-type	n = 5	30 µM DHT	40,30,35,30,35	100,93,94,83,85	91	7	90,86,77,76,65	79	10	100,93,94,83,85	0,7,6,17,15	Pictured in Fig. 3
zip9 mosaic mutant	n = 5	30 µM DHT	25,30,40,40,36	80,96,95,95,83	90	8	97,83,72,87,75	83	10	80,96,95,95,83	3,4,5,5,17	Pictured in Fig. 3
Wild-type	n = 5	30 µM DHT	36,29,35,36,30	88,79,85,97,76	85	8	75,86,85,80,93	84	7	88,79,85,97,76	12,14,15,3,7	Pictured in Fig. 3
hcar1-4 mosaic mutant	n = 5	30 µM DHT	33,36,35,36,35	90,88,82,80,88	86	4	72,91,94,83,100	88	11	90,88,82,80,88	10,9,6,17,0	Pictured in Fig. 3
wild-type	n = 8	30 µM Testosterone	90,75,82,53,59,42,53,50	51,56,62,56,69,66,88,68	65	11	0,0,0,0,0,0,0,0	0	0	0,0,0,0,0,0,0,0	49,44,38,44,31,34,12,32	Pictured in Fig. 3
gprc6a mosaic mutant	n = 8	30 µM Testosterone	164,87,90,81,73,96,72,88	34,35,42,39,47,60,51,53	45	9	0,0,0,0,0,0,0,0	0	0	0,0,0,0,0,0,0,0	65,65,58,52,50,40,49,47	Pictured in Fig. 3
ahr2 mosaic mutant	n = 4	30 µM Testosterone	48,72,34,48	72,70,67,68	69	2	0,0,0,0,0	0	0	0,0,0,0,0	28,30,33,32	Pictured in Fig. 3
Wild-type	n = 5	30 µM Testosterone	34,60,50,68,60	73,66,72,75,66	70	4	0,0,0,0,0	0	0	0,0,0,0,0	27,34,28,25,34	Pictured in Fig. 3
zip9 mosaic mutant	n = 5	30 µM Testosterone	60,95,96,95,48	70,70,71,76,89	75	8	0,0,0,0,0	0	0	0,0,0,0,0	30,30,29,24,11	Pictured in Fig. 3
Wild-type	n = 5	30 µM Testosterone	58,47,48,48,49	70,70,83,79,81	77	6	0,0,0,0,0	0	0	0,0,0,0,0	30,30,17,21,19	Pictured in Fig. 3
hcar1-4 mosaic mutant	n = 5	30 µM Testosterone	96,82,48,48,48	72,75,87,75,79	78	6	0,0,0,0,0	0	0	0,0,0,0,0	28,25,13,25,21	Pictured in Fig. 3

Table 2. Embryo data accompanying Figure 4. Wild-type embryos were injected with Cas9 protein without any gRNAs

Genotype	Clutch (biological replicate)	Treatment	Number of embryos/clutch	% Cardiac edema, 3 dpf	Mean % embryos with cardiac edema	Standard deviation (cardiac edema)	% Tail curvature, 3 dpf	Mean % embryos with tail curvature	Standard deviation (tail curvature)	% Cardiac edema + tail curvature, 3 dpf	% Normal embryos, 3 dpf	Notes
Wild-type	n = 10	0.1% DMSO	12,16,10,14,20,22,10,12,10,12	0,0,0,0,0,0,0,0,0,0	0	0	0,0,0,0,0,0,0,0,0,0	0	0	0,0,0,0,0,0,0,0,0,0	100,100,100,100,100,100,100,100,100,	Pictured in Fig. 4
heterozygous *gprc6a*	n = 10	0.1% DMSO	20,30,20,31,42,42,20,22,24,22	0,0,0,0,0,0,0,0,0,0	0	0	0,0,0,0,0,0,0,0,0,0	0	0	0,0,0,0,0,0,0,0,0,0	100,100,100,100,100,100,100,100,100,	Pictured in Fig. 4
homozygous *gprc6a*	n = 10	0.1% DMSO	14,16,10,18,20,20,10,12,11,12	0,0,0,0,0,0,0,0,0,0	0	0	0,0,0,0,0,0,0,0,0,0	0	0	0,0,0,0,0,0,0,0,0,0	100,100,100,100,100,100,100,100,100,	Pictured in Fig. 4
Wild-type	n = 6	15 µM androstanedione	20,21,20,26,18,25	88,70,80,100,100,92	88	12	90,85,100,100,100,92	95	6	88,70,80,100,100,92	10,15,0,0,0,8	Pictured in Fig. 4
heterozygous *gprc6a*	n = 6	15 µM androstanedione	50,46,40,51,38,39	75,80,90,100,100,93	90	10	90,86,96,94,100,95	94	5	75,80,90,100,100,93	10,14,4,0,0,5	Pictured in Fig. 4
homozygous *gprc6a*	n = 6	15 µM androstanedione	18,17,18,21,15,19	72,76,,90,100,100,88	88	12	94,76,100,100,100,100	95	10	72,76,,90,100,100,88	6,24,0,0,0,0	Pictured in Fig. 4
Wild-type	n = 6	30 µM DHT	20,17,24,19,18,21	90,100,100,100,100,100	98	4	81,78,100,100,100,100	93	11	90,100,100,100,100,100	10,0,0,0,0,0	Pictured in Fig. 4
heterozygous *gprc6a*	n = 6	30 µM DHT	50,42,54,42,42,36	95,100,100,100,100,94	98	3	85,82,90,100,100,96	92	8	95,100,100,100,100,94	5,0,0,0,0,4	Pictured in Fig. 4
homozygous *gprc6a*	n = 6	30 µM DHT	22,19,21,23,25,22	92,95,100,100,100,100	98	3	78,85,86,100,100,90	90	9	92,95,100,100,100,100	8,5,0,0,0,0	Pictured in Fig. 4
Wild-type	n = 13	30 µM Testosterone	15,26,25,12,28,16,27,23,21,26,14,20,23	73,71,65,66,81,84,72,92,68,82,92,75,73	76	9	0,0,0,0,0,0,0,0,0,0,0,0,0	0	0	0,0,0,0,0,0,0,0,0,0,0,0,0	27,29,35,34,19,16,28,8,32,18,8,27,27	Pictured in Fig. 4
heterozygous *gprc6a*	n = 13	30 µM Testosterone	38,44,43,24,50,48,45,52,57,41,38,50,48	73,77,61,79,75,85,65,90,77,82,84,70,68	76	8	0,0,0,0,0,0,0,0,0,0,0,0,0	0	0	0,0,0,0,0,0,0,0,0,0,0,0,0	27,23,39,21,25,15,35,10,23,18,16,30,32	Pictured in Fig. 4
homozygous *gprc6a*	n = 13	30 µM Testosterone	19,26,22,12,18,32,24,21,18,29,20,26,25	52,61,46,50,62,65,36,66,62,66,70,60,56	58	10	0,0,0,0,0,0,0,0,0,0,0,0,0	0	0	0,0,0,0,0,0,0,0,0,0,0,0,0	48,39,54,50,38,35,64,34,38,34,35,40,44	Pictured in Fig. 4
Wild-type	n = 13	30 µM Testosterone	15,26,25,12,28,16,27,23,21,26,14,20,23	73,71,65,66,81,84,72,92,68,82,92,75,73	76	9	0,0,0,0,0,0,0,0,0,0,0,0,0	0	0	0,0,0,0,0,0,0,0,0,0,0,0,0	27,29,35,34,19,16,28,8,32,18,8,27,27	Pictured in Fig. S4
heterozygous *gprc6a* $^{bcm53/+;\ bcm52/+}$	n = 2	30 µM Testosterone	38,44	73,77	75	2	0,0	0	0	0,0	27,23	Pictured in Fig. S4
homozygous *gprc6a* $^{bcm53/-;\ bcm52/-}$	n = 2	30 µM Testosterone	19,26	52,61	57	5	0,0	0	0	0,0	48,39	Pictured in Fig. S4
heterozygous *gprc6a* $^{bcm56/+;\ bcm54/+;\ bcm55/+}$	n = 4	30 µM Testosterone	43,24,50,48	61,79,75,85	75	9	0,0,0,0	0	0	0,0,0,0	39,21,25,15	Pictured in Fig. S4
homozygous *gprc6a* $^{bcm56/-;\ bcm54/-;\ bcm55/-}$	n = 4	30 µM Testosterone	22,12,18,32	46,50,62,65	56	8	0,0,0,0	0	0	0,0,0,0	54,50,38,35	Pictured in Fig. S4
heterozygous *gprc6a* $^{bcm56/+;\ bcm54/+}$	n = 5	30 µM Testosterone	45,52,57,41,38	65,90,77,82,84	80	8	0,0,0,0,0	0	0	0,0,0,0,0	35,10,23,18,16	Pictured in Fig. S4
homozygous *gprc6a* $^{bcm56/-;\ bcm54/-}$	n = 5	30 µM Testosterone	24,21,18,29,20	36,66,62,66,70	60	12	0,0,0,0,0	0	0	0,0,0,0,0	64,34,38,34,35	Pictured in Fig. S4
heterozygous *gprc6a* $^{bcm59/+;\ bcm58/+}$	n = 3	30 µM Testosterone	50,44,46	70,81,76	75	5	0	0	0	0	30,18,23	Pictured in Fig. S4
homozygous *gprc6a* $^{bcm59/-;\ bcm58/-}$	n = 3	30 µM Testosterone	26,23,23	60,60,65	61	2	0	0	0	0	53,39,34	Pictured in Fig. S4
heterozygous *gprc6a* $^{bcm61/+;\ bcm60/+}$	n = 3	30 µM Testosterone	48,40,50	68,87,86	80	10	0	0	0	0	32,12,14	Pictured in Fig. S4
homozygous *gprc6a* $^{bcm61/-;\ bcm60/-}$	n = 3	30 µM Testosterone	25,22,20	56,59,55	56	2	0	0	0	0	44,40,44	Pictured in Fig. S4

Table 3. Embryo data accompanying Figure 6 and Figure S5. The same data are pooled and grouped by gene (top table) or not pooled and grouped by allele (bottom table)

Genotype	Clutch (biological replicate)	Treatment	Number of embryos/clutch	% Cardiac edema, 3 dpf	Mean % embryos with cardiac edema	Standard deviation (cardiac edema)	% Tail curvature, 3 dpf	% Cardiac edema + tail curvature, 3 dpf	% Normal embryos, 3 dpf	Notes
Wild-type	n = 6	0.1% DMSO	30,40,28,32,25,25	0,0,0,0,0,0	0	0	0,0,0,0,0,0	0,0,0,0,0,0	100,100,100,100,100,100,	Pictured in Fig. 5
Wild-type	n = 3	5 µM Calindol	40,38,40	0,0,0	0	0	0,0,0	0,0,0	100,100,100	Pictured in Fig. 5
Wild-type	n = 3	5 µM NPS-2143	30,30,30	0,0,0	0	0	0,0,0	0,0,0	100,100,100	Pictured in Fig. 5
Wild-type	n = 3	100 µM EGCG	40,40,40	0,0,0	0	0	0,0,0	0,0,0	100,100,100	Pictured in Fig. 5
Wild-type	n = 6	30 µM Testosterone	50,59,63,47,52,57	62,59,71,78,73,70	69	7	0,0,0,0,0,0	0,0,0,0,0,0	38,41,29,22,27,37	Pictured in Fig. 5
Wild-type	n = 6	5 µM Calindol + 30 µM Testosterone	50,55,59,51,57,44	76,60,74,78,61,72	70	8	0,0,0,0,0,0	0,0,0,0,0,0	24,40,26,22,39,28	Pictured in Fig. 5
Wild-type	n = 6	5 µM NPS-2143 + 30 µM Testosterone	50,59,64,57,55,65	50,42,43,43,25,33	39	9	0,0,0,0,0,0	0,0,0,0,0,0	50,58,57,57,75,67	Pictured in Fig. 5
Wild-type	n = 6	100 µM EGCG + 30 µM Testosterone	50,61,67,43,48,67	42,34,28,27,22,40	32	8	0,0,0,0,0,0	0,0,0,0,0,0	59,66,72,73,78,67	Pictured in Fig. 5
gprc6a $^{bcm56/-;\ bcm54/-;\ bcm55/-}$	n = 4	0.1% DMSO	26,20,34,22	0,0,0,0,0	0	0	0,0,0,0,0	0,0,0,0,0	100,100,100,100	Pictured in Fig. 5
gprc6a $^{bcm56/-;\ bcm54/-;\ bcm55/-}$	n = 3	5 µM NPS-2143	20,30,30	0,0,0	0	0	0,0,0	0,0,0	100,100,100	Pictured in Fig. 5
gprc6a $^{bcm56/-;\ bcm54/-;\ bcm55/-}$	n = 3	100 µM EGCG	30,40,28	0,0,0	0	0	0,0,0	0,0,0	100,100,100	Pictured in Fig. 5
gprc6a $^{bcm56/-;\ bcm54/-;\ bcm55/-}$	n = 4	30 µM Testosterone	25,18,21,26	48,50,42,38	45	5	0,0,0,0	0,0,0,0	52,50,58,62	Pictured in Fig. 5
gprc6a $^{bcm56/-;\ bcm54/-;\ bcm55/-}$	n = 4	5 µM NPS-2143 + 30 µM Testosterone	25,24,30,19	52,50,53,63	55	5	0,0,0,0	0,0,0,0	48,50,47,37	Pictured in Fig. 5
gprc6a $^{bcm56/-;\ bcm54/-;\ bcm55/-}$	n = 4	100 µM EGCG + 30 µM Testosterone	26,22,24,24	42,40,50,54	47	6	0,0,0,0	0,0,0,0	58,60,50,46	Pictured in Fig. 5

Table 4. Embryo data accompanying Figure 7.

Genotype	Clutch (biological replicate)	Treatment	Number of embryos/clutch	% Cardiac edema, 3 dpf	Mean % embryos with cardiac edema	Standard deviation (cardiac edema)	% Tail curvature, 3 dpf	% Cardiac edema + tail curvature, 3 dpf	% Normal embryos, 3 dpf	Notes
Wild-type	n = 4	0.1% DMSO	20,20,11,20	0,0,0,0	0	0	0,0,0,0	0,0,0,0	100,100,100,100	Pictured in Fig. 6
Wild-type	n = 4	30 μM Estradiol	42,30,26,22	0,0,0,0	0	0	0,0,0,0	0,0,0,0	100,100,100,100	Pictured in Fig. 6
Wild-type	n = 4	30 μM Testosterone	28,33,41,41	89,75,95,82	85	9	0,0,0,0	0,0,0,0	11,25,5,18	Pictured in Fig. 6
Wild-type	n = 4	0.1% DMSO	20,25,24,19	0,0,0,0	0	0	0,0,0,0	0,0,0,0	100,100,100,100	Pictured in Fig. 6
MZcyp19a1b ^{uab124}	n = 4	0.1% DMSO	20,20,20,10	0,0,0,0	0	0	0,0,0,0	0,0,0,0	100,100,100,100	Pictured in Fig. 6
Wild-type	n = 4	30 μM Testosterone	35,27,21,26	94,88,80,76	85	8	0,0,0,0	0,0,0,0	6,12,20,24	Pictured in Fig. 6
MZcyp19a1b ^{uab124}	n = 4	30 μM Testosterone	28,26,29,28	89,84,75,78	82	6	0,0,0,0	0,0,0,0	11,16,25,22	Pictured in Fig. 6
Wild-type	n = 4	0.1% DMSO	12,10,12,14	0,0,0,0	0	0	0,0,0,0	0,0,0,0	100,100,100,100	Pictured in Fig. 6
heterozygous *esr1a* $^{uab118/+}$	n = 4	0.1% DMSO	25,24,23,28	0,0,0,0	0	0	0,0,0,0	0,0,0,0	100,100,100,100	Pictured in Fig. 6
homozygous *esr1a* $^{uab118/-}$	n = 4	0.1% DMSO	12,12,12,12	0,0,0,0	0	0	0,0,0,0	0,0,0,0	100,100,100,100	Pictured in Fig. 6
Wild-type	n = 4	30 μM Testosterone	24,26,19,27	70,80,78,77	76	4	0,0,0,0	0,0,0,0	30,20,22,23	Pictured in Fig. 6
heterozygous *esr1a* $^{uab118/+}$	n = 4	30 μM Testosterone	44,50,39,45	65,86,71,71	73	9	0,0,0,0	0,0,0,0	35,14,29,29	Pictured in Fig. 6
homozygous *esr1a* $^{uab118/-}$	n = 4	30 μM Testosterone	23,22,20,22	69,90,75,81	79	9	0,0,0,0	0,0,0,0	31,10,25,19	Pictured in Fig. 6
Wild-type	n = 4	0.1% DMSO	10,13,11,14	0,0,0,0	0	0	0,0,0,0	0,0,0,0	100,100,100,100	Pictured in Fig. 6
heterozygous *esr2a* $^{uab134/+}$	n = 4	0.1% DMSO	20,25,18,29	0,0,0,0	0	0	0,0,0,0	0,0,0,0	100,100,100,100	Pictured in Fig. 6
homozygous *esr2a* $^{uab134/-}$	n = 4	0.1% DMSO	11,12,12,12	0,0,0,0	0	0	0,0,0,0	0,0,0,0	100,100,100,100	Pictured in Fig. 6
Wild-type	n = 4	30 μM Testosterone	30,30,25,30	70,70,84,80	76	7	0,0,0,0	0,0,0,0	30,30,16,20	Pictured in Fig. 6
heterozygous *esr2a* $^{uab134/+}$	n = 4	30 μM Testosterone	52,57,56,67	73,80,82,86	80	5	0,0,0,0	0,0,0,0	27,20,18,14	Pictured in Fig. 6
homozygous *esr2a* $^{uab134/-}$	n = 4	30 μM Testosterone	30,39,25,30	66,84,84,83	79	9	0,0,0,0	0,0,0,0	34,16,16,17	Pictured in Fig. 6
Wild-type	n = 4	0.1% DMSO	11,11,13,10	0,0,0,0	0	0	0,0,0,0	0,0,0,0	100,100,100,100	Pictured in Fig. 6
heterozygous *esr2b* $^{uab128/+}$	n = 4	0.1% DMSO	18,22,27,20	0,0,0,0	0	0	0,0,0,0	0,0,0,0	100,100,100,100	Pictured in Fig. 6
homozygous *esr2b* $^{uab128/-}$	n = 4	0.1% DMSO	12,12,12,12	0,0,0,0	0	0	0,0,0,0	0,0,0,0	100,100,100,100	Pictured in Fig. 6
Wild-type	n = 4	30 μM Testosterone	24,30,36,47	87,80,88,85	85	4	0,0,0,0	0,0,0,0	13,20,12,15	Pictured in Fig. 6
heterozygous *esr2b* $^{uab128/+}$	n = 4	30 μM Testosterone	76,61,67,80	77,77,86,82	81	4	0,0,0,0	0,0,0,0	23,23,14,18	Pictured in Fig. 6
homozygous *esr2b* $^{uab128/-}$	n = 4	30 μM Testosterone	32,26,33,34	84,80,84,90	85	4	0,0,0,0	0,0,0,0	16,20,16,10	Pictured in Fig. 6

Table 5. Embryo data accompanying Figure 8. Experiments within horizontal lines were performed together.